THESIS ON NATURAL AND EXACT SCIENCES B45

Structural and Electrical Properties of Spray Deposited Copper Indium Disulphide Films for Solar Cells

ARVO MERE

TALLINN 2006

TALLINN UNIVERSITY OF TECHNOLOGY

Faculty of Chemistry and Materials Technology

Department of Materials Science
Chair of Semiconductor Materials Technology

Dissertation was accepted for the commencement of the degree of Doctor of Philosophy in Natural and Exact Sciences on February 6, 2006

Supervisor: Research Professor Malle Krunks, Department of Materials Science

Opponents: Professor Dieter Meissner, University of Applied Sciences, Wels, Austria
Professor Jaak Kikas, University of Tartu, Estonia

Commencement: March 17, 2006, at 14.00,
Lecture hall: VII-131,
Tallinn University of Technology, Ehitajate tee 5, Tallinn

Declaration: Hereby I declare that this doctoral thesis, my original investigation and achievement, submitted for the doctoral degree at Tallinn University of Technology has not been submitted for any degree or examination.

Arvo Mere

ISSN 1406-4723
ISBN 9985-59-604-8

Doktoritöö loodusteadustes

Pihustussadestatud Vaskindium Disulfiidi Kilede Struktuursed ja Elektrilised Omadused ning Rakendus Päikesepatareides

ARVO MERE

TALLINN 2006

TALLINNA TEHNIKAÜLIKOOL

Keemia- ja materjalitehnoloogia teaduskond

Materjaliteaduse Instituut
Pooljuhtmaterjalide tehnoloogia õppetool

Doktoritöö on vastu võetud avalikuks kaitsmiseks loodusteaduste doktori kraadi taotlemiseks 06. veebruaril 2006.a.

Juhendaja: Uurija-Professor Malle Krunks, Materjaliteaduse Instituut

Oponendid: Professor Dieter Meissner, Tehnoloogia Ülikool, Wels, Austria
Professor Jaak Kikas, Tartu Ülikool, Eesti

Avalik kaitsmine: 17. märts, 2006, kell 14.00,
Auditoorium: VII-131,
Tallinna Tehnikaülikool, Ehitajate tee 5, Tallinn

Deklaratsioon: Käesolevaga deklareerin, et minu doktoritöö on minu originaalne töö ja on teostatud Tallinna Tehnikaülikoolis ning seda pole kunagi varem esitatud teaduskraadi taotlemiseks või väitlemiseks.

Arvo Mere

Allkiri

LIST OF PUBLICATIONS

The thesis is based on the following papers, which are referred to in the text by Roman numerals **I-VIII**:

I. M. Krunks, V. Mikli, O. Bijakina, H. Rebane, **A. Mere**, T. Varema, E. Mellikov, Composition and structure of $CuInS_2$ films prepared by spray pyrolysis, *Thin Solid Films*, 361-362 (2000) 61-64.

II. M. Krunks, O. Kijatkina, J. Blums, I. Oja, **A. Mere**, E. Mellikov, Cost-effective sprayed $CuInS_2$ films for solar cells, *Proceedings 17-th European PVSEC*, Oct. 22-26, 2001, Munich, Germany, published by WIP-Munich and ETA-Florence, v.2 (2002) 1211-1214.

III. A. Mere, O. Kijatkina, H. Rebane, J. Krustok, M. Krunks, Electrical properties of sprayed $CuInS_2$ films for solar cells, *J. Phys. Chem. Solids*, 64 (2003) 2025-2029.

IV. A. Mere , A. Katerski, O. Kijatkina, M. Krunks, 2004, Solar Cell Structures by Non -Vacuum Techniques Based on Sprayed $CuInS_2$ Absorber Layers. - *Proceedings 19-th PVSEC*, June 7-11, 2004, Paris, 1973-1976.

V. M. Krunks, O. Kijatkina, **A. Mere**, T. Varema, I.Oja, V. Mikli, Sprayed $CuInS_2$ films grown under Cu-rich conditions as absorbers for solar cells, *Solar Energy Materials and Solar Cells*, 87 (2005) 207-214.

VI. I. Oja, M. Nanu, A. Katerski, M. Krunks, **A. Mere**, J. Raudoja, A. Goossens, Crystal quality studies of $CuInS_2$ films prepared by spray pyrolysis, *Thin Solid Films*, 480-481 (2005) 82-86.

VII. M. Krunks, **A. Mere**, A. Katerski, V. Mikli, J. Krustok, Characterisation of sprayed $CuInS_2$ films annealed in hydrogen sulphide atmosphere, *Thin Solid Films,* In Press, Corrected Proof, Available online 19 January 2006, at http.//www.sciencedirect.com/.

VIII. M. Krunks, **A. Mere**, O. Kijatkina, Solar Cell Based on $CuInS_2$ Absorber Layer Prepared by Chemical Spray Pyrolysis, *United States Patent Application Publication* No: US 2005/0271827 A1, Dec. 8, 2005.

Author's own contribution

The contribution by the author to the papers included in the thesis is as follows:

- **I.** XRD measurements, analysis, minor part of writing.
- **II.** Optical and electrical measurements, analysis, minor part of writing.
- **III.** XRD measurements and analysis, electrical measurements and analysis, major part of writing.
- **IV.** Electrical measurements, analysis, major part of writing.
- **V.** XRD measurements, analysis, minor part of writing.
- **VI.** XRD measurements and analysis, Raman spectroscopy results analysis, major part of writing.
- **VII.** XRD measurements and analysis, electrical and optical measurements, analysis and major part of writing.
- **VIII.** Electrical measurements, analysis, minor part of writing.

Deposition, chemical and thermal treatments of the films, SEM, EDX, different chemical analyses and Raman spectroscopic measurements were done by coworkers.

List of abbreviations and symbols

AC	alternative current
ALD	atom layer deposition
AM	air mass
CA	Cu-Au ordering
CBD	chemical bath deposition
CH	chalcopyrite
CIGSe	$CuInGaSe_2$
CIS	$CuInS_2$
CISCuT	CIS on Cu-tape
CISe	$CuInSe_2$
Cu-Pt	copper platinum ordering
DC	direct current
EDX	energy dispersive X-ray microanalysis
E_g	optical bandgap
EPFL	Ecole Polytechnique Federale de Lausanne
FF	fill factor
FhG-ISE	Fraunhofer Institute for Solar Energy Systems
FTIR	Fourier Transform Infra-Red
FWHM	full width half maximum
ILGAR	Ion-Layer-Gas-Reaction Process
ITO	indium tin oxide
JCPDS	Joint Committee on Powder Diffraction Standards
j_{SC}	short circuit current
KCN	potassium cyanide
NIR	near infrared
NREL	National Renewable Energy Laboratory
PDF	powder diffraction file
RT	room temperature
RTP	rapid thermal process
SEM	scanning electron microscopy
UNSW	University of New South Wales
UV-VIS	ultraviolet visible
V_{oc}	open circuit voltage
XPS	x-ray photoelectron spectroscopy
XRD	x-ray diffraction
η	efficiency of solar cell
Φ_b	barrier height of the p-n junction

Table of contents

Introduction

Photovoltaic (PV) literally means light-electricity: photo comes from the Greek *pho*s, meaning light, and volt from the Italian scientist *Alessandro Volta*; a pioneer in the study of electricity. PV technology, originally developed for space applications in the 1950-s, has many advantages: it is modular, clean, silent, easy to maintain, and can be installed almost anywhere. The electricity produced can be used directly, stored locally or fed into an existing electricity grid [1].
The first efficient solar cell based on crystalline silicon was developed at Bell Labs in 1954 [2]. Although silicon is not the ideal material for photovoltaic conversion due to its low absorption ability together with the complicated manufacture and high cost of crystalline silicon, at present PV market is mainly based on various forms of crystalline silicon [3] . In 2004, nearly 85% of world's PV cell and module production was based on sliced single crystal and polycrystalline silicon [4].
Photovoltaic cell and module production in the world increased in 2004 to 1195 MW representing a 57% increase compare to 2003 (716MW) [4]. Today's photovoltaic market is still far away from noticeable contribution to the world energy consumption [3], although the production forecast for the year 2010 is 4000 MW/year [4]. The price of standard PV modules is currently approximately 3 € /W. A continuos drop in prices is preplanned – to 2 € /W by 2010, up to 0.5 € /W in 2030. After 2030 a further price reduction is expected [1, 4] only if its costs can be lowered, that photovoltaic electricity could become a competitive source of energy [1].
Technology Research Advisory Council (PV-TRAC) at the EU Commission declared its mission to support rapid development of world-class, cost–competitive European photovoltaics for sustainable electricity production and delivery of electricity on a large scale at a competitive cost [1].
A key factor in reducing of the cost of modules is connected with the manufacturing processes used.
From this point of view the technologies can be categorised as:

1) Options primarily aimed at very low cost (while optimising efficiency).
2) Options primarily aimed at very high efficiency (while optimising cost).

My doctoral thesis could be classified as belonging to the first category, because $CuInS_2$ as a solar cell material has been prepared by the low cost spray pyrolysis technique. The aim was to characterise some physical properties of sprayed $CuInS_2$ thin films and evaluate their suitability for solar cells.

1. Literature review and aim of the work

1.1. Thin film solar cells

Thin film solar cells are considered as an alternative to commercially available but expensive crystalline silicon solar cells. The most successful thin film solar cells belong to one of the following materials families [5].
(i) the CIGS family, where the absorbing semiconductor consists of $CuInSe_2$ or a related I-III-VI_2 type material or alloy, such as $CuInS_2$, $Cu(In,Ga)Se_2$ or $Cu(In,Ga)(S,Se)_2$;
(ii) the CdTe family;
(iii) the silicon family, consisting of an amorphous or microcrystalline silicon–hydrogen alloy
(a-Si:H or μc-Si:H) or related alloys, such as a-SiGe:H or a-SiC:H.

Table 1.1.
Output characteristics of the best solar cells in laboratories [6]

Structure	Voc, mV	J_{SC}, mA/cm^2	FF, %	η , %	Organisation
Monocrystalline Si	706	42.2	82.8	24.7	UNSW
Polycrystalline Si	664	37.7	80.9	20.3	FhG-ISE
Amorphous Si	887	19.4	74.1	12.7	Sanyo
ZnO/CdS/CIGS	693	35.7	79.4	19.5	NREL
CdS/CdTe	843	25.09	74.5	15.8	Univ.South Florida NREL
Nanocrystalline TiO2/Dye	795	19.4	71.0	11.0	EPFL

Nevertheless, relatively high efficiencies have been achieved in laboratories (Table 1.1), commercial panels show conversion efficiencies about two times lower (Table 1.2).
Table 1.2.
Comparison of conversion efficiencies (in %) of laboratory cells and commercial panels [7]

Material type	Best lab cell S ≅ 1 cm^2	Best panel cell S ≅ 1000 cm^2	Commercial panel
c-Si	24.7		10–15
CIGS	19.2	13.4	6–8
CdTe	16.5	10.7	10
α-Si	14.5	10.4	6–8

1.2. Solar cells based on I-III-VI_2 type absorbers

I-III-VI_2 type chalcopyrite materials have already demonstrated to be potential candidates for large-scale productions. The typical structure of a solar cell is presented in Fig. 1.1. The highest efficiencies up to now have been achieved on $CuInSe_2$ (CISe) based cells with Ga/Ga+In ratio of 25-30 % (CIGSe), corresponding to a bandgap of approximately 1.2 eV [8]. However, CISe technologies also pose some problems. In order to achieve high efficiencies, the adjustment of stoichiometry and incorporation of other elements, such as Ga, S, Na are necessary, which increase the production costs. From the environmental point of view, the presence of selenium and the steps of selenization, in some cases also in the H_2Se atmosphere, are problematic.

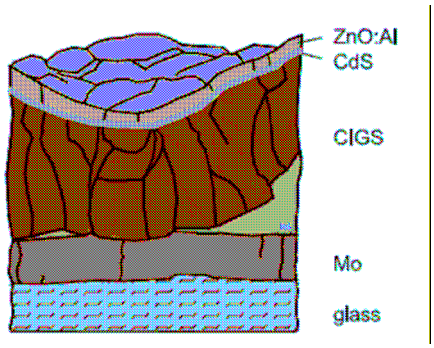

Fig. 1.1. Typical structure of the CIGS (CIS) based solar cell [9]

$CuInS_2$ (CIS) belongs to the family of I-III-VI_2 materials, being one of the most promising chalcopyrite absorbers due to a bandgap of 1.5 eV, which lies in optimum range for solar energy conversion [10]. The absorbers with a larger bandgap are favoured for the production of highly efficient single cells with large open circuit voltages and top cells in the tandem systems [11]. CIS based cells show improved blue response, lower efficiency loss at operating temperature and higher radiation stability than the devices of low bandgap absorbers [12, 13]. Non-toxic constituent elements are important from the environmental point of view. CIS cells are not affected by the outdiffusion of Na from the glass [14]. This avoids the requirement for the utilisation of Na diffusion barriers or the fair control of the incorporation of Na, as in the case of CISe films. The considerations above and the rapid thermal process (RTP) of Cu-excess growth are believed to make the production of CIS cells scaleable, fast and economic [11, 10, 15].
$CuInS_2$ as an absorber layer material for the thin film solar cell has the highest theoretical solar energy conversion efficiency of 28.5% among Cu-chalcopyrite absorber materials [8]. Although according to fundamental considerations, the CIS

cells are expected to show efficiencies superior to those of CIGSe cells, sulfide has reached efficiencies of 11.4 % [16] and 12.5 % [11], which is about 60% of efficiency of the selenides up to now. This is mostly due to the significantly lower open circuit voltage as compared to the bandgap in the case of CIS. The lowered open circuit voltage is a result of the specific feature of the ZnO/CdS/$CuInS_2$ heterojunction band diagram (Fig.1.2). The interface states between the CdS/$CuInS_2$ interface cause the cliff-like band bending and open the recombination path for photogenerated electron-hole pairs through the interface states at the CdS/$CuInS_2$ interface [17]. The CISe based solar cell with similar layers configuration shows spike-like band bending of the conduction band, and the absorber is inverted from p-type to n-type close to the interface. As a result, the interface recombination is suppressed and bulk recombination is dominant in CISe cells [17]. Therefore, in the case of the CIS absorber layer investigators of thin films solar cells are faced with a greater challenge.

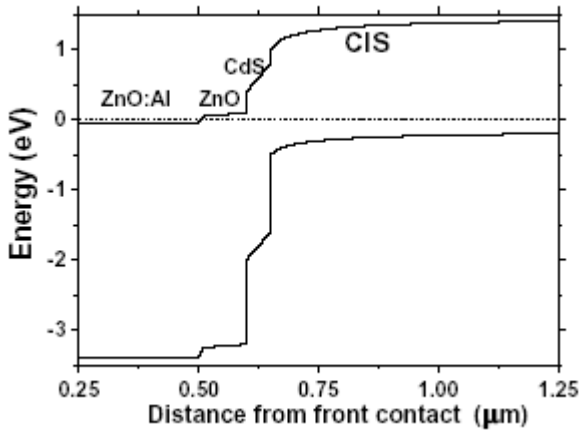

Fig. 1.2. Band diagram of a ZnO/CdS/$CuInS_2$ heterojunction [17].

1.3. Phase equilibrium in the Cu-In-S system and polymorphism in $CuInS_2$

The equilibrium in the Cu-In-S system is only partially known due to its complexity. The Gibbs phase triangle diagram of the Cu-In-S system at room temperature (Fig. 1.3) shows a possible coexistance of $CuInS_2$ with other compounds in the thermodynamical equilibrium. At room temperature, stable phases in the Cu-S system are CuS, $Cu_{1.75}S$, $Cu_{1.96}S$, Cu_2S, in the In-S system In_2S_3, In_6S_7 and InS. In the Cu-In-S system, two ternary compounds could be formed – $CuInS_2$ and $CuIn_5S_8$. $CuInS_2$ exists in three modifications (chalcopyrite, zincblende, wurtzite) depending on the temperature, $CuIn_5S_8$ has a cubic spinel structure over the whole temperature range from 20 ºC up to the melting point at 1085 ºC [19].

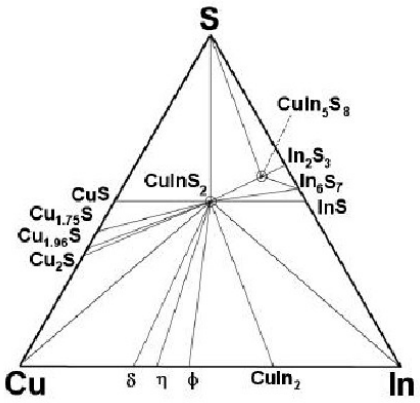

Fig. 1.3. Gibbs phase triangle of the Cu-In-S system at RT [20, 21].

$CuInS_2$ preferably has a stable chalcopyrite structure [20]. The lattice type is primitive tetragonal, the corresponding space group is $I\bar{4}2d$, its mineral name is roquesite and the lattice parameters are: a=5.523Å, c=11.141Å (PDF 27-0159). Although I-III-VI_2 compounds normally crystallise in the chalcopyrite structure (space group $I\bar{4}2d$), other crystalline structures may exist in accordance with the Grimm-Sommerfeld rule. According to this rule, different structures can be obtained by changing the stacking sequence of cations. Cations stacking sequences in the [102] and [111] directions lead to the so-called Cu-Au (space group $P\bar{4}m2$) or Cu-Pt ordered structures [13]. Cu-Au and Cu-Pt ordering is named by the arrangement of atoms in the corresponding metallic superstructures.

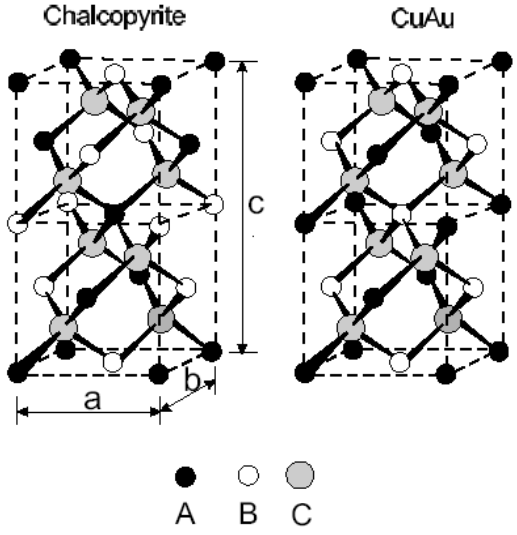

Fig. 1.4 Chalcopyrite and CuAu-ordered unit cells. A-Cu, B-In, C-S [13].

If the formation energy of those cation orderings is quite close to the chalcopyrite one, it may result in the formation of metastable domains in a crystal. According to the theoretical calculations the formation energy difference between the chalcopyrite and Cu-Au ordering in $CuInS_2$ is very small (2 meV/atom) and thus the probability of coexisting is high [23]. For $CuInSe_2$ the difference is larger (9 meV/atom) [23]. The crystal structures of the chalcopyrite and Cu-Au ordered phases are presented in Fig.1.4. Also, the bandgap energy of Cu-Au ordered phase is 30 meV lower than the bandgap energy of the chalcopyrite [24]. It has been shown in different studies that the presence of Cu-Au ordered phase in the absorber layer is unwanted, leading to an inferior quality of the solar cells [25, 26, 27].
A conventional XRD study is usually incapable of detecting the presence of Cu-Au ordered structure due to the overlapping of almost all XRD peaks [13]. The Raman spectroscopy is an approved method to study qualitative and quantitative contribution of the chalcopyrite and Cu-Au ordered phases in CIS [13, 20, 28, 29], as well as possible secondary phases [30].
CIS chalcopyrite and Cu-Au ordered phase detection by the Raman spectroscopy can be based on only few most intense, dominant bands in the Raman pattern. Chalcopyrite phase is detected by a symmetric A_1 mode at 290 cm^{-1} [13, 20, 25, 29]. The Cu-Au ordered phase could be detected by 305 cm^{-1} band and additionally, by the weak 60 cm^{-1} band [13]. The band broadening carries information about the Raman active domain size [29]. Raman spectroscopic characterization has been applied for CIS films obtained by various deposition methods except spray pyrolysis.

1.4. Deposition techniques of CIS thin films

Several preparation methods are used for a systematic investigation of the material properties relevant to photovoltaic application. Vacuum-based processes could be divided into two main classes [11]:
1) simultaneous evaporation (co-evaporation) of elements with defined metal flux ratios, maintaining an excess of sulphur pressure at substrate temperatures of 400-600°C [17, 31, 32, 33]; 2) sequential processes comprising sputtering or evaporation of metal films followed by sulfurisation in sulphur
and/or H_2S atmosphere; or sequential evaporation or sputtering of binary precursors and sulfurisation in different sulphur sources [10, 11, 15, 34-39]. Two-step processes are evaluated due to their superior potential for industrial production. Rapid thermal processing (RTP) allows a significant decrease in the processing time, cells based on RTP may reach the efficiency of 11.4 % [16]. Their common feature is that the best absorber material is usually grown under the Cu-excess conditions leading to secondary Cu-S phases, which has an important role in the films growth mechanism.
To reduce the production costs of CIS, the technologies of CISCuT (CIS on Cu-tape) [40] and wet chemical deposition routes such as electrodeposition [41], ILGAR [42] and chemical spray pyrolysis [5, 19, 43- 56] have been developed.

Solar cells based on CIS by CISCuT technique have reached the efficiencies of 9% [40], electrodeposition – 1.3 % and spray - 0.6-2% (Table 1.3).

1.5. Properties of spray deposited CIS films

Chemical spray pyrolysis process for deposition of thin films

Chemical spray pyrolysis (CSP) is a process where a precursor solution is pulverised in the form of small droplets onto the preheated substrate, where upon the chemical reaction (usually thermal decomposition), a film of thermally more stable compound forms. The chemical reactants should be selected so that the products other than the desired compound are volatile at the temperature of deposition [57].

CSP is a convenient, low-cost, and rapid method of depositing large-area thin films. This technique has been successfully applied to prepare metal oxide thin films. Since the pioneering work by Chamberlin and Skarman in 1966 on CdS [58], it has been applied to deposit different binary and ternary chalcogenide films.

- ***Formation of CIS films***

The formation chemistry of CIS films in the spray pyrolysis process has been studied by M. Krunks *et al*. [59-62]. In spray deposition process, using $InCl_3$, $CuCl_2$ and $SC(NH2)_2$ as precursor materials in an aqueous solution, CIS forms from binary sulfides of Cu_xS and In_2S_3 [59, 63, 64]. The lowest deposition temperature is determined by the decomposition temperature of the copper–thiourea complex above 250 °C. The upper limit for the growth temperature is around 400 °C as at higher temperatures oxidation occurs and in addition to CIS by XRD the In_2O_3 phase was detected [62].

- ***Phase and elemental composition, structure and optical properties of sprayed CIS films***

CIS films prepared at low deposition temperatures around 300 °C contain a high amount of residues, such as chlorine, carbon and nitrogen issued from precursors [65]. The content of residues decreases and the crystallinity of the sprayed CIS films increases by the deposition temperature [65]. At temperatures above 400 °C, in addition to CIS the In_2O_3 phase forms if deposited in air [62]. Thus, CIS films could be prepared in quite narrow temperature region of 350-380 °C and the compromise between the film purity and oxidation processes must be made, as was shown by O. Kijatkina [64].
The molar ratio of Cu, In and S precursor materials in spray solution has a considerable influence on the film properties. The S/Cu higher than two was found necessary to cover the deficiency of chalcogen in deposited films [66, 67], the Cu/In ratio has an influence on the structure and crystallinity. According to XRD and SEM studies [48, 67], CIS and CISe films prepared from “In-rich” solutions

have been found to be multiphase [64, 67, 68, 69]. It has been reported that In_2S_3 or In_2Se_3 are a secondary phases in the CIS or CISe films, respectively [70, 69]. In contrast, Brown et al. attributed extra peaks in the diffractogram of $CuInSe_2$ films to the phases of $Cu_{2-x}Se$ and Cu_2Se [68]. The use of "Cu-rich" solutions (mainly Cu/In = 1.1) results in the (112) direction orientated CIS films with an increased crystallite size and a secondary $Cu_{2-x}S$ phase, which segregates on the surface of the films and can be easily removed by KCN etching [64]. Concerning the optical properties, the absorption coefficient α, in the range of $10^4 - 10^6$ cm^{-1} and optical direct bandgap in the range of 1.38-1.45 eV were measured for sprayed CIS films [5, 54, 62, 64, 66, 70- 72].

- ***Properties of treated CIS films***

Post-deposition thermal treatments of sprayed CIS films in an inert or reducing (H_2, H_2S) atmospheres at temperatures 400- 500 ºC lead to the improvement of structural properties and show a significant purification effect [65]. Treatments improve film crystallinity (films grown from the solutions with the Cu/In=1.0), but there was no effect on the films grown from In-rich solutions [65]. By treatments in vacuum or an inert atmosphere, the *p* – type conductivity of sprayed CIS films changed into the *n* – type independent of the solution composition. The observed change of the conductivity type has been explained by the formation of the conductive In_2O_3 phase and supported by the loss of sulphur during the annealing [73, 64]. It has been found that post-deposition treatments in hydrogen or hydrogen sulfide atmosphere are more effective to reduce the residues content (including oxygen), whereas the sprayed films preserve the p-type conductivity [65, 64].
Annealing of CIS films at 380 ºC in sulphur atmosphere improves crystallinity and purity, but decreases the conductivity from 10^{-1} to 10^{-3} $\Omega^{-1}cm^{-1}$ [74].

- ***Electrical properties of sprayed CIS films***

Studies of electrical properties are scarce [67, 74-76]. It has been found that the resistivity of as-deposited films depends on the Cu/In ratio in the solution and changes from about 10^3-10^5 Ω·cm to about 10^{-1}-10^{-2} Ω·cm with an increase in the Cu/In ratio in the spray solution. High resistivity has been explained by poor film crystallinity. Low resistivities are characteristic of the films deposited with an excess of copper and are attributed to the presence of highly conductive $Cu_{2-x}S$ phase segregated at grain boundaries. In all the studies the p-type conductivity has been reported present in sprayed CIS films. The Hall mobility was found to be lower than 10 $cm^2/V{\cdot}s$ even for the films prepared from Cu-rich solutions [70]. No publications cover the concentration of carriers in sprayed CIS films. The conductivity temperature dependent measurements have been performed only for sulphur-annealed CIS films to investigate possible conductivity mechanisms [74].

1.6. Solar cells based on sprayed CIS and related compounds

According to the literature survey, the works published in this field could be divided into two different time periods. The first period started in the 1980s, in 1990s the interest dropped due to relatively low efficiencies (2-3%) achieved on solar cells based on sprayed Cu-ternary absorbers. The second period started at the end of the 1990s.

The first attempts to prepare CIS and CISe thin films by spray pyrolysis were made in 1979 by Pamplin *et al.* [77]. The first working solar cell by the spray technique based on ZnO/$CuInSe_2$ heterostructure with a conversion efficiency of 2 % was prepared in 1982 [22]. Studies on sprayed CISe based cells were continued by Duchemin *et al.* [78- 80]. It was found that the deposition of bilayer CISe (In-rich and Cu-rich) instead of single-layer CISe onto the ITO/CdS:Al, CdS leads to a significant increase in the current density [78]. The optimisation of the deposition parameters of the ITO/CdS:Al, CdS/ CISe (In-rich), CISe (Cu-rich) structure allows for an increase in the efficiency of up to 3.3 % and 4 % [79, 80]. The use of ZnO window layer (ITO/ZnO/CdS/CISe) results in lowered output parameters: V_{oc}=250 mV and j=11.5 mA/cm^2 [80]. Results concerning superstrate configuration sprayed CISe cells are summarised in Table 1.3.

Table 1.3 Summary of solar cells based on sprayed CIS or CISe

Absorber	Structure	Cell output parametres	Year	Ref.
CISe	ITO/ZnO/$CuInSe_2$	η= 2 %	1982	[22]
CISe	ITO/CdS:Al, CdS/CISe	V_{oc}=250 mV, j_{SC}=6 mA/cm^2	1986	[78]
CISe	ITO/CdS:Al, CdS/ CISe (In-rich)/CISe (Cu-rich)	V_{oc}=273 mV, j_{SC}=23 mA/cm^2 FF=0.45, η= 3.3 %	1987	[79]
CISe	ITO/CdS:Al, CdS/ CISe (In-rich)/ CISe (Cu-rich) ITO/ZnO/CdS/CISe	η= 4 % V_{oc}=250 mV, j_{SC}=11.5 mA/cm^2	1989	[80]
CIS	ZnO:In/CIS interl., CIS (Cu-rich)/Al, annealing in vaacuum	V_{oc}=280mV, jsc = 13.3mA/cm^2 FF = 0.38, η= 2 %	1987	[46]
CISSe	ITO/ n-CdZnS:In/p-$CuIn(S_{0.5}Se_{0.5})_2$	V_{oc}= 325 mV, j_{SC}= 10.3 mA/cm^2 FF=0.33, η=1.1 %	1994	[81]
CIS	Mo/CIS/CdS/ZnO/Al	V_{oc}=304 mV, j_{SC}=5.25 mA/cm^2, FF=0.29, η= 0.68%	2003	[72]
CIS	ITO/CdS/CIS	η= 0.65%	2005	[44]

Concerning CIS, the all-sprayed $CuInS_2$/SnOx structure exhibits an efficiency of 3% [5]. The formation of a heterojunction in this system could be argued, as in following studies the CIS/SnOx contact was found to be ohmic. It is quite possible that Al used for contacting forms a Schottky barrier with CIS. All-layers-sprayed CIS solar cells were developed by Tiwari *et al.* [46] (Table 1.3). The bilayer absorber was prepared similarly to the procedure reported for CISe cells in [78] , whereas the composition and properties of bilayer CIS were not reported [46]. It was mentioned that the deposition of an interlayer of CIS and post-deposition annealing of junctions were essential to obtain a solar cell efficiency of 2 % [46] .
By spray K**.** Subbaramaiah *et al.* prepared a backwall configuration heterojunction of p-CuIn $(S_{0.5}Se_{0.5})_2$ /n-CdZnS:In with an efficiency of 1.1 % in 1994 [81]. Efficiency recorded was considerably lower than that previously reported for CIS and CISe based solar cells prepared by spray. The first set of investigations on solar cells by the spray technique were directed to prepare the working cell, no sufficient attention was paid to material properties and technology.
Starting from the 1990s, studies in the field of spray pyrolysis deposition were initiated, interest was shifted to the development of properties of the films, especially structural and optical properties [54, 62, 64, 70-72]. Only in a few works the authors prepared and characterised the solar cell [44, 72]. The efficiencies of the sprayed CIS cell remain below 1 % (Table 1.3). No other characterisation of a solar cell, except the output parameters of the cell have been published.

1.7. Aim of the thesis

1.7.1. Summary of the literature overview

The studies of sprayed $CuInS_2$ films and solar cells can be summarised as follows:

- The main part of the studies of CIS films, prepared by spray pyrolysis is devoted to structural and optical characterisation, depending on the deposition parameters, main attention is paid to CIS films deposited from slightly copper-rich solutions.
- The use of Cu-rich spray solutions results in $CuInS_2$ films where Cu_xS phase segregates onto the film surface and can be removed by chemical etching. There is no clear concept of the phase composition of the films deposited from In-rich solutions. Also, the effect of highly Cu-rich solutions on film crystallinity and morphology has been poorly studied. The investigations of differently ordered structures in sprayed CIS films are absent.
- Only some studies cover the effect of post-deposition thermal treatments on the film properties.

- The electrical properties of spray-deposited films have been studied scarcely, being limited to carriers' type, some works report the conductivity measurements.
- Solar cells based on sprayed Cu-ternary absorber are covered by a limited number of publications, whereby the characterisation of solar cells is restricted to cell output parameters only.

1.7.2. Goals of the research

On the basis of the current state sprayed CIS film studies and the tasks set for solar cell development by cost-effective deposition techniques, the objectives of the doctoral thesis were to study:

1. the phase composition and crystallinity of spray-deposited copper indium disulphide films depending on the Cu/In molar ratio in the solution;
2. the effect of annealing in the hydrogen sulphide atmosphere on the phase composition, crystallinity and optical properties of sprayed CIS films;
3. the $CuInS_2$ structure ordering in as-deposited and annealed in hydrogen sulphide atmosphere films;
4. electrical parameters, such as conductivity and carriers' concentration in as-deposited and annealed in hydrogen sulphide atmosphere CIS films;
5. the sprayed $CuInS_2$ absorber layer based solar cells depending on the Cu/In molar ratio in the CIS spray solution and the buffer layer type.

2. Experimental

2.1. CIS films deposition and preparation of solar cells

CIS films deposition parametres by the spray technique, film post-deposition treatment conditions, and the preparation of Schottky barriers or solar cells are described in the published papers [I-VII].

2.2. Characterisation of CIS films and solar cells

The characterisation methods of CIS films and solar cells, the used set-up and devices, measurement parametres and formulas and their applicability conditions are summarised as follows below.

Structural and optical characterisation

Structural properties of $CuInS_2$ films were determined by XRD, Micro Raman spectroscopy, VIS-NIR spectroscopy and SEM. Main focus was on the examination of the phase composition and crystal quality of the sprayed CIS films.

- **XRD**

XRD patterns of the deposited films were recorded on AXS D5005 diffractometer (Tallinn University of Technology), using monochromatic Cu Kα radiation (λ=1.540560 Å), anode voltage 40 kV, anode current 40 mA, θ-θ regime, step θ=0.04 deg or θ=0.02 deg, counting time 2-10 s per step and sample rotation. The diffractograms were analysed by the evaluation program EVA 3.0 of the package Diffrac Plus Basic from Bruker Analytical X-ray Systems. The phases were identified using the JCPDS files.
The crystallite size was calculated from the FWHM of the (1 1 2) XRD peak of $CuInS_2$ at 2θ=27.8741 deg (PDF 27-0159) using Scherrer formula 3.1.

- **SEM, EDX**

The LEO SUPRA and Jeol JSM-840A instruments (Tallinn University of Technology) were used to study the surface morphology and cross-section of the films and solar cells. The thickness of the films was also derived from SEM cross section images. The elemental composition of the films was studied by the X-ray microanalysis (EDX) on a Link Analytical AN 10000 spectrometer, using the accelerating voltage 7 kV and the beam current 3 nA. EDX measurements were made from the surface area of 2 mm^2 at four different characteristic points.

- **Micro Raman spectroscopy**

Experimental Micro Raman setup (Delft University of Technology) was used to obtain information about the polymorpfous phases of $CuInS_2$. Excitation wavelength was 532 nm, the beam power density was 0.05 MW/cm^2. The criteria for the power density were established by the thermal widening of the band at 290 cm^{-1}. The Raman sensitive depth was about 150 nm. The SPEX340E monochromator was used for spectrum recording at RT.

- **VIS-NIR spectroscopy**

Absorbance and transmittance spectra of the films were recorded on VARIAN TECHTRON MODEL 636 and FTIR SPECTRUM GX spectrometer from PERKIN ELMER Company (Tallinn University of Technology). The absorption coefficient and the bandgap of the CIS films were calculated according to the Eqs. 3.2. and 3.3.

Electrical characterisation

Electrical measurements were made for the CIS films deposited onto glass and ITO covered glass substrates, for the CIS/Al Schottky barriers and solar cells structures. Various contact materials and configurations were used. Graphite and sputtered Au were used as ohmic contacts for/to CIS. The Schottky barriers on CIS were prepared by the evaporation of aluminium with an area of 1.83 mm^2 on top of the CIS layer. The ITO layer was used as a back contact.

- **Hot probe measurements**

The experimental set-up (Tallinn University of Technology) was used as an express method to determine the conductivity type of the sprayed films.

- **Current-voltage characteristics**

DC measurements were performed using an AUTOLAB PGSTAT 30 set-up (Tallinn University of Technology).
The resistivity of the CIS film was calculated according to Eq. 2.1, whereas the resistance (R) was calculated from the I-V curve [82].

$$\rho = \frac{R \cdot A}{d}, \text{ where} \qquad (2.1)$$

A- cross section area of the current flow channel,
d- length of the current flow channel,
R- resistance between the contacts.
The temperature dependent conductivity was measured in the temperature interval 200–400 K using a vacuum cryostat to set the temperature.

I-V curves of solar cells were measured in dark and under the white light illumination of
100 mW/cm^2. The solar cell efficiency was calculated by Eq. 2.2 [82].

$$\eta = \frac{j_{SC} \cdot V_{OC} \cdot FF}{P_{st}} \cdot 100\%, \text{ where} \qquad (2.2)$$

η - efficiency,
j_{SC} - short circuit current density,
V_{OC} –open circuit voltage,
FF- fill factor,
P_{st} – power of the standard illumination *of* AM1.5 (100 mW/cm^2)

The fill factor of the solar cell was calculated by Eq. 2.3 [82].

$$FF = \frac{j_{eff} \cdot V_{eff}}{j_{SC} \cdot V_{OC}}, \text{ where} \qquad (2.3)$$

FF- fill factor,
j_{eff} -current density at maximum power output,
V_{eff} -voltage at maximum power output,
V_{OC} –open circuit voltage,
j_{SC} - short circuit current density

The solar cell series resistance and shunt resistance were calculated according to Eqs. 2.4 and 2.5, respectively.

$$R_s = \frac{\Delta V}{\Delta I}, \text{ where} \qquad (2.4)$$

R_s - serial resistance,
ΔV - voltage difference on the I-V curve,
ΔI - current difference on the I-V curve

$$R_{sh} = \frac{\Delta V_0}{\Delta I_0}, \text{ where} \qquad (2.5)$$

R_{sh} - shunt resistance of solar cell,
ΔV_0 - voltage difference on the I-V curve at I=0,
ΔI_0 - current difference on the I-V curve at V=0

The ideality factor of the solar cell diode was calculated from the linear part of the lnj versus V curve at RT by Eq. 2.6 [83].

$$n = \frac{q}{k \cdot T} \cdot \frac{d(V - I \cdot R_s)}{d(\ln I)}, \text{ where} \qquad (2.6)$$

n - diode ideality factor,
q – electron charge $1.6 \cdot 10^{-19}$ C,
k - Boltzman's factor $1.38 \cdot 10^{-23}$ J/K,
T- absolute temperature,
V - applied voltage,
I - current,
R_S - serial resistance of the diode

- **Admittance spectroscopy**

Admittance measurements were performed on AUTOLAB PGSTAT 30 set-up (Tallinn University of Technology).
The concentration of majority carriers was calculated according to Eq. 2.7 using C-V measurement data and the Mott-Schottky model [82]. C-V measurements were performed at the frequency of 1 kHz.

$$N = \frac{2}{q \cdot \varepsilon \cdot \varepsilon_0 \cdot A^2} \cdot \frac{dV}{d(\frac{1}{C^2})} \text{ , where} \qquad (2.7)$$

N- effective concentration of carriers,
q – electron charge $1.6 \cdot 10^{-19}$ C,
ε=10.2 (permittivity of CIS)
$\varepsilon_0 = 8{,}85 \cdot 10^{-12}$ F/m,
A -Schottky barrier area,
V - applied reverse DC voltage,
C – junction capacitance
Admittance spectroscopy was also used to determine the photogenerated electron hole recombination paths in the solar cell in the frequency range of 10Hz-1MHz and at applied AC voltage of 20 mV. The following circuit model diagram (Fig. 2.1.) was used to calculate solar cell capacitance.

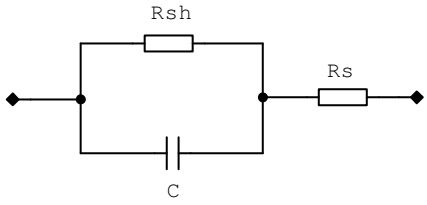

Fig. 2.1. Circuit model of solar cell, *Rsh*- shunt resistance, *Rs*- series resistance, *C*- capacitance of solar cell.

The capacitance of this circuit was calculated according to Eq. 2.8 [82].

$$C = \frac{Z'}{\left[(Z' - R_S)^2 + Z''^2\right]\omega} \text{ , where} \qquad (2.8)$$

Z'- measured frequency dependent real part of the impedance,
Z''- measured frequency dependent imaginary part of the impedance,
R_S - serial resistance acquired from I-V curve,
ω- scanned angular frequency.
The temperature dependent and bias dependent admittance measurements were performed at various temperatures (160-300K). The bias dependent admittance measurements verified the activation energy belonging to the interface states.The activation energy of the dominant interface states at the interface of the p-n junction was calculated according to Eq. 2.9.

$$\omega_i = \xi \cdot T^2 \cdot \exp(-\frac{E_a}{kT}) \text{, where} \qquad (2.9)$$

ω_i - inflection point of the C-ω curve,
ξ - temperature independent part of the pre-exponent,
T- absolute temperature,
E_a - dominant interface states energy,
k - Boltzman's factor

3. Results and discussion

3.1. Phase composition and structural properties of spray deposited CIS films

Photovoltaic applications require that the $CuInS_2$ absorber layer be of chalcopyrite structure, orientated in the (112) direction, having large grains and p-type of conductivity with the concentration of carriers of $1 \cdot 10^{16}$ - $1 \cdot 10^{17}$ 1/cm^3 [75, 84-87]. In the present work two methods - XRD and Raman spectroscopy- have been used to determine the phase composition and structural properties of spray deposited CIS films. The sensitivity of the X-ray powder diffraction technique is approximately 2 mass % for the secondary crystalline phases if overlapping of the diffraction peaks is absent. The overlapping of the XRD patterns is also the limit of the method. For example, the determination of the metastable Cu-Au ordered structure of the $CuInS_2$, which is the unwanted phase of the CIS-type absorber materials [20, 28, 88] is out of the scope of a conventional XRD method. Consequently, the XRD method and Raman spectroscopy are both important methods to determine the structure and crystal quality of the absorber layer.

3.1.1. Phase composition and crystallinity of CIS films depending on the Cu/In molar ratio in spray solution by XRD

The effect of the precursors molar ratio (Cu/In) in a spray solution on the phase composition and crystallinity of the films was studied for the films deposited at 360- 380 ^{0}C. The main criteria to choose this deposition temperature were: no formation of oxide phases was observed [59], the lowest amount of chlorine, carbon and nitrogen residues in as-deposited films [65].
The results of XRD characterisation of as-sprayed films are reported in papers [I, II, III, V, VI]

- *Films from In-rich solutions*

According to XRD (Fig.3.1), the films prepared from "In-rich" (Cu/In = 0.8, 0.9) as well as from "1:1:3" (Cu/In=1.0) solutions show poor crystallinity. The films from In-rich solution (Cu/In=0.8) show only two replica at 2θ=26.5 and 46.4 deg (Fig.3.1). A strong reflection at 2θ= 46.4 deg, obviously belonging to the (220) plane of $CuInS_2$ phase (JCPDS PDF27-0159), was also observed in spray chemical vapor deposited CIS films [72].

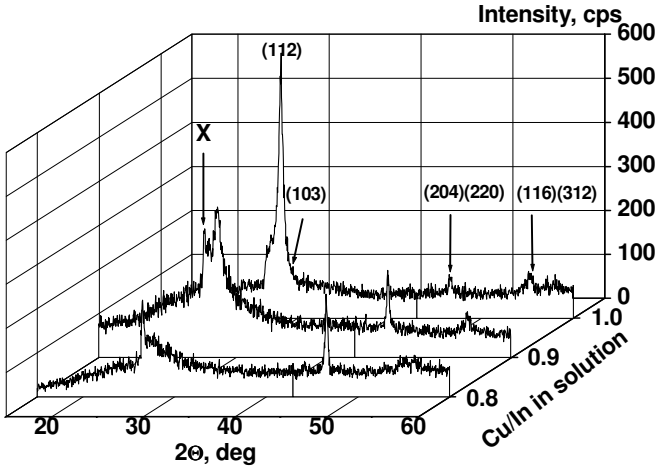

Fig. 3.1. XRD patterns of as-deposited CIS films prepared at 370 ^{0}C using the In-rich spray solutions (Cu/In=0.8-1.0).

The (112) peak of $CuInS_2$ is not shaped out in the case of In-rich solutions. An extra XRD reflection in the low-angle shoulder of the $CuInS_2$ (112) peak at 2θ = 26.5 deg does not belong to the $CuInS_2$ phase (marked by "X" in Fig. 3.1). This reflection was recorded in CIS films prepared by spray pyrolysis [70, 89] and by spray chemical vapour deposition [72, 90].

We believed that an organic phase could be present as well [I]. In a later study of our group [65] it was shown that the amount of organic residues was lower than 5 mass % at deposition temperatures above 320 °C. Additionally, the extra peak was recorded in the films heat treated at 500 °C in H_2 atmosphere with an insignificant amount of organic residues [65]. Thus, the extra peak unlikely corresponds to the organic phase. The extra reflection in the low-angle shoulder of the (112) peak of $CuInS_2$ was also recorded in CIS films prepared from Cu-In precursor [91, 92], where the organic phase cannot be present. In the case of CIS, by the sulfurization of Cu-In precursors and by electrodeposition, the extra peak was assigned to an In-rich ternary $CuIn_{11}S_{17}$ [92]. It has been reported that CIS films prepared by ALD under Cu-poor conditions result in the mixture of $CuInS_2$ and $CuIn_5S_8$ spinel phase [28]. $CuIn_5S_8$ phase was also indentified in CIS films prepared on the Cu tape (CISCuT) [93] and in (Ag, Cu) InS2 films prepared by the diffusion of Cu, Ag and S into the In_xS precursor layer [94].

Taking into account the literature data on CIS films prepared by different techniques as well as the phase diagram of the Cu-In-S system [19, 20], an another

ternary compound could be expected to be responsible for the extra reflection at the low-angle shoulder of (112) peak of $CuInS_2$. Thus, the peak at $2\theta = 26.5$ deg could belong to the $CuIn_5S_8$ phase (PDF 72-096), but cannot be identified only by the XRD because of only some diffraction peaks in the pattern (Fig.3.1). However, the extra reflection is absent in the case of Cu-rich solutions (Fig.3.2). The speculation on the presence of the $CuIn_5S_8$ phase should be proved by another characterization technique, for instance, by Raman spectroscopy measurements. The identification of a secondary ternary in the film is highly important as the possible $CuIn_5S_8$ phase is an n-type semiconductor with the optical bandgap of 1.31 eV [95] and accordingly undesirable if p-type absorber is to be deposited.

- ***Films from Cu-rich solutions***

The use of Cu-rich spray solutions (Cu/In=1.1-4.0) results in a CIS film where all the appearing diffraction peaks are belonging to the $CuInS_2$ phase (JCPDS PDF 27-0159) and the films are highly (112) orientated (Fig. 3.1).

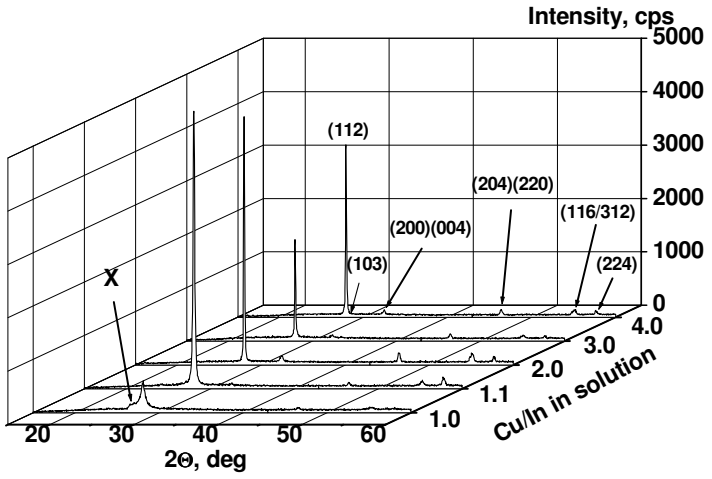

Fig. 3.2. XRD patterns of as-deposited CIS films prepared at 370 ^{0}C using Cu-rich spray solutions (Cu/In=1.1-4.0). XRD pattern of the film deposited at Cu/In=1.0 in spray solution is presented for comparison.

According to XRD, it could be proposed that films are of chalcopyrite structure, as a weak (103) reflection and splitting of the (004)/(002), (220)/(204) and (312)/(116) reflections, characteristic of the chalcopyrite structure [67, 67, 94], are observed. The extra reflection at $2\theta = 26.5$ deg is absent in the XRD patterns of the films deposited from Cu-rich solutions. Consequently, the secondary phase, which one was present in the films prepared from In-rich solutions, is not present in those films.

- ***Crystallite size in as-sprayed CIS films depending on the Cu/In molar ratio in spray solution***

The FWHM of the $CuInS_2$ peak at 2θ=27.97 deg (plane 112) was used to calculate the average crystallite size in the film, using Sherrer's formula (Eq. 3.1) [96].

$$< D >= \frac{k \cdot \lambda}{(B - b)\cos\theta}, \text{ where} \qquad (3.1)$$

<*D*>- average crystallite size,
k- Shape factor (in these calculations spherical crystallite shape was assumed and k=1),
λ- x-ray radiation wavelength,
B- FWHM of the measured peak,
b- FWHM of the closest peak of the crystallite standard,
θ- Diffraction angle of the measured peak.
The results are published in [II, V] and a summary is presented as a bar graph in Fig. 3.3.

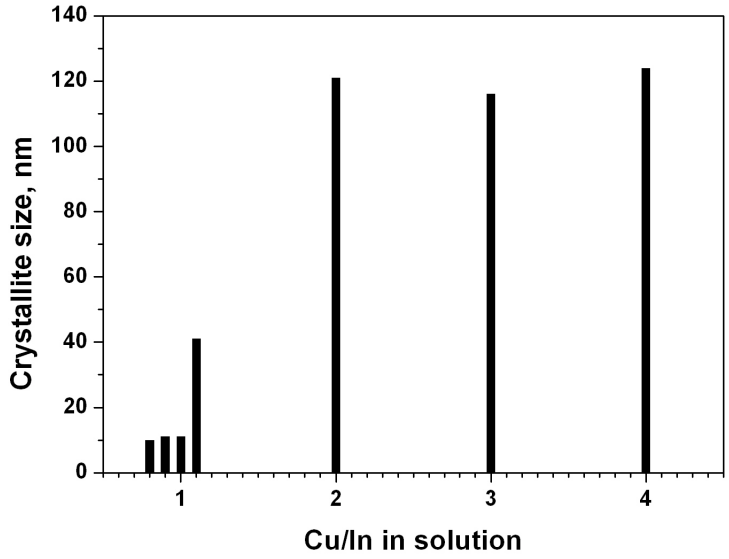

Fig. 3.3. The average crystallite size of CIS films deposited at 370 °C, depending on the Cu/In molar ratios in the spray solution.

The crystallite size of 10 nm, 40 nm and 120 nm was calculated for the films at the Cu/In ratios of 1.0, 1.1 and 2.0 in the solution, respectively. The molar ratios of Cu/In >2 in the spray solution have an insignificant effect on the mean crystallite

size. It could be seen that the deposition of In-rich solutions results in the films consisting of nanosize crystallites, whereas Cu-rich solutions lead to the films with a mean crystallite size above 100 nm.
The effect of the Cu/In molar ratio in the spray solution on the film surface morphology and optical properties will be discussed in section 3.2. Although the use of Cu-rich solutions results in $CuInS_2$ films consisting of crystallites with a size larger than 100 nm, there are two specific characteristics which can make use of these kind of layers in thin film solar cells questionable. Firstly, the films prepared from Cu-rich solutions are not dense in the region of large grains after KCN etching, which removes the CuxS phase (See Fig. 3.2.2 in section 3.2.1). The observed feature offers favourable conditions for the electrical shunts when the solar cell structure will be developed. Secondly, large grains in the CIS films deposited from Cu-rich solutions exhibit an In-rich composition according to EDX [V, 64].

3.1.2. Characterisation of sprayed and annealed in hydrogen sulphide atmosphere CIS films by XRD and electron beam techniques

This part focuses on the effect of post-deposition treatment in hydrogen sulfide (H_2S) atmosphere at temperatures above 500 ºC onto the structural properties of sprayed CIS films. Results of the studies are published in [VI, VII].

- ***XRD study of CIS films annealed in H_2S atmosphere***

Treatment in the H_2S atmosphere at 525 °C for two hours followed by rapid cooling leads to well-crystallised (112) orientated $CuInS_2$ films (Figs. 3.4 and 3.5) without the extra replica at $2\theta = 26.5$ deg. The appearance of the (103) reflection and splitting of the (004)/(200) and (204)/(220) reflections are distinctly observed in the case of Cu/In=1.0 (Fig. 3.4) and refer to the presence of the chalcopyrite structure [69]. Similar structural improvement is detected for the "In-rich" films after the heat-treatment at temperatures higher than 500 °C (Fig. 3.5). However, inconsiderable differences, such as unresolved (004) reflection and very weak unidentified reflection at $2\theta = 26.9$ deg, are still present.
Our results obtained for the films sprayed at $Cu/In \leq 1$ are in good agreement with the results recorded for Cu-poor films prepared by ALD and heat treated in the H_2S atmosphere at 500 °C [91]. It was proposed that $CuIn_5S_8$ transforms into $CuInS_2$ and In_2S_3, whereby In_2S_3 evaporates during the annealing [91].
Our results show that treatment time of one or two hours as well the cooling rate (slow or rapid) has an insignicant effect on the XRD patterns of annealed films (See also Fig. 1 in [VII]).
The crystallite size was calculated from (112) peak at XRD diffractograms. The calculations show that the crystallite size of sprayed $CuInS_2$ films upon the heat treatment at 525 °C for two hours followed by rapid cooling is about 90 nm,

independent of the Cu/In in spray solution. The use of an annealing time of 60 minutes and a slow cooling, the average crystallite size is 98 nm. The most significant growth of crystallites is observed for the films from "In-rich" solutions as the crystallite size lower than 10 nm is increased by the factor of ten. In contrast, for the films from Cu-rich solutions, an increase by the factor of two was observed. Therefore it is supposed that the removal of the secondary ternary phase together with improved chemical purity will develop favourable conditions for the crystallite growth.

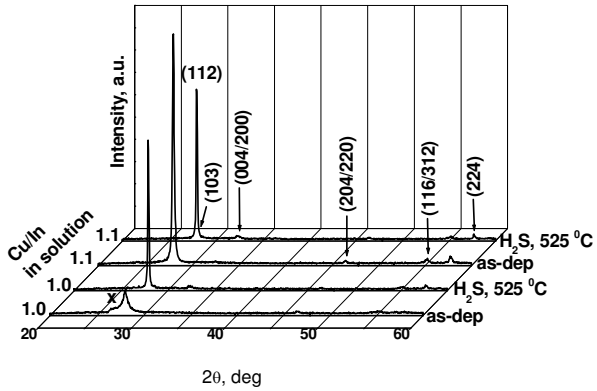

Fig. 3.4. XRD patterns of as-sprayed and annealed in flowing H_2S atmosphere at 525 °C (2 h, rapid cooling) $CuInS_2$ films, deposited at Cu/In= 1.0-1.1 in spray solution.

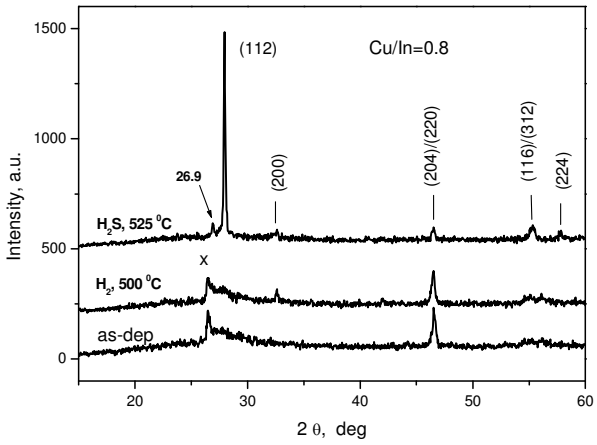

Fig. 3.5. XRD patterns of as-sprayed and annealed in flowing H_2S atmosphere at 525 °C (2 h, rapid cooling) $CuInS_2$ films, deposited at Cu/In= 0.8 in spray solution.

- ***SEM and EDX study of CIS films annealed in the H_2S atmosphere***

The development of grains in films by H_2S annealing is characterised by the SEM cross-sectional micrographs (Fig. 3.6.). According to SEM, an as-deposited film (from the solution with Cu/In=1.0) shows a columnar structure and the grain size is about 20 nm (Fig. 3.6. a). Upon annealing the grain size increases significantly, the film comprises grains with sizes up to 300 nm on the preserved ITO electrode (Fig. 3.6. b). The results of SEM on grain size correspond to those recorded by XRD for crystallite size.

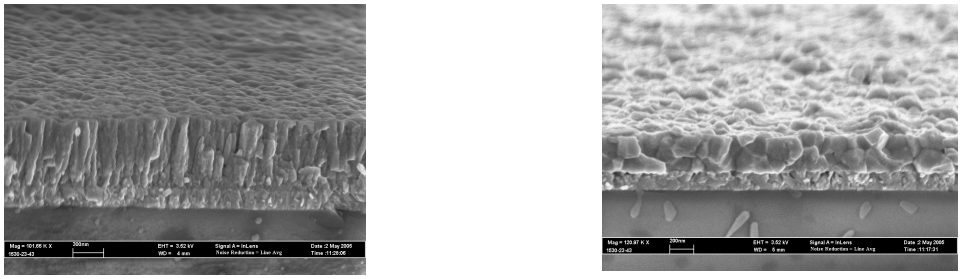

a) b)

Fig. 3.6. SEM cross-sectional micrographs of CIS films deposited from "stoichiometric" (Cu/In=1.0) solutions: a) as-deposited; b) annealed for 60 minutes at 530 °C in flowing H_2S atmosphere and subjected to slow cooling.

By annealing, significant changes could be observed in the film elemental composition. The deficiency in sulphur (Table 1) and contamination with chlorine with an amount of about 1.5 mass. % are characteristic of as-deposited films. The results are in compliance with the literature data [65, 74, VI]. Upon H_2S treatment, the content of sulphur is significantly increased and the chlorine is not detectable by EDX. The films on glass substrate exhibit nearly stoichiometric composition whereas on ITO covered glass a slightly In-rich composition was observed (Table 3.1). In the latter case the impact of indium from ITO electrode is not excluded. The elemental composition of the films from "Cu-rich" solutions is not affected by the treatment time and cooling rates.

Table 3.1.
Elemental composition by EDX of CIS films as-sprayed and annealed in H_2S atmosphere, as a function of the treatment temperature, time and cooling conditions

Substr.	Cu:In:S In sol.	Anneal.temp. C/time, min	Coo-ling	Cu, at.%	In, at.%	S, at.%	Cl, mass%	Cu/ In	S/ (Cu+In)
Glass	1:1:3	-	-	28.0	25.0	43.6	1.95	1.12	0.82
Glass	1:1:3	450/120	R	25.9	25.7	44.4	0.7	1.01	0.86
Glass	1:1:3	530/120	R	25.79	24.51	49.70	<0.1	1.05	0.99
Glass	1.1:1:3.15	530/120	R	24.67	25.28	50.05	<0.1	0.98	1.00
ITO	1.1:1:3.15	530/60	R	24.76	26.04	49.07	<0.1	0.95	0.97
ITO	1.1:1:3.15	530/60	S	24.34	26.08	49.48	<0.1	0.93	0.98

R-rapid, S-slow cooling

3.1.3. Characterisation of sprayed CIS films by Raman spectroscopy

Results of Raman spectroscopy studies of sprayed CIS films are published in [VI].

Raman spectra of as-sprayed KCN etched films prepared at different Cu/In molar ratios in the spray solution are presented in Fig. 3.7. The films deposited from "In-rich" solution exhibit lower scattering intensity, which could be caused by a higher density of defects. Lower crystallinity of CIS films from "In-rich" solutions has been shown by XRD (See 3.1.1). Raman spectra of the CIS films were fitted with Lorentzians as shown for the films from In-rich solutions (Fig. 3.7. c). In addition to the A_1 modes of the CH and CA structures, several E/B_2 modes of the CH-ordered compound were taken into account in the fitting procedure. The obtained results show that the most intensive Raman band consists of two bands, A_1 band of CH ordered compound at 290 cm^{-1} and A_1^* band of CA ordering at 300 cm^{-1}. The intensity of the A_1^* mode of Cu-Au ordered phase is higher compared to the A_1 mode of CH ordering. However, the position of these bands was observed to be independent of the Cu/In in spray solution (Fig.3.7).

In addition to the Raman bands of the CH and CA ordered $CuInS_2$ at 290 and 300 cm^{-1}, accordingly, CIS films grown from In-rich solution contain an intensive Raman band at around 340 cm^{-1} (Fig.3.7.c). The intensity of the 340 cm^{-1} band is comparable to that of the CA and CH bands of $CuInS_2$. The band can be subtracted into three sub-bands, as shown in Fig. 3.7. c. The low frequency modes at 321 and 338 cm^{-1} could belong to the B_2^1 and E^1_{LO} modes of the chalcopyrite structure, respectively [97]. The mode at 348 cm^{-1} could belong to the $CuIn_5S_8$ phase [97, 98]. The observation that the Raman peak at 348 cm^{-1} vanishes together with the extra reflection at $2\theta = 26.5$ in the XRD pattern (Figs. 3.1 and 3.2) by increasing the Cu/In in solution supports the assumption of the CIS phase formation. Furthermore, the formation of $CuIn_5S_8$ spinel phase is also reported in CIS films prepared by ALD under Cu-poor conditions [74], in $(Ag,Cu)InS_2$ thin films prepared by the diffusion of Cu, Ag and S into In_xS precursor layer [99] as well in

the films prepared by the CISCuT (CIS on Cu tape) technique [98]. Speculations related to the formation of $CuIn_5S_8$ phase in addition to $CuInS_2$ phase in the case of deposition of In-rich solutions are sustained by the post-deposition thermal treatments and will be discussed hereinafter.

Fig. 3.8. shows the Raman spectra of CIS films after the heat treatment in the H_2S environment at 525 °C for 2 hours. It can be seen that after the heat treatment Raman bands are narrower than in as-deposited films (Fig. 3.7). The intensity of A_1 band (CH phase) has increased as compared to A_1^* band (CA ordered phase) (Fig. 3.8.). However, no shift in the spectral position of A_1 CH mode as compared to as-deposited films was detected.

Another important change in the spectra, especially for films sprayed from In-rich solution, is the vanishing the Raman band located at 348 cm^{-1}, which could have belonged to $CuIn_5S_8$. The behaviour observed is in correlation with the XRD results showing upon annealing the disappearance of an extra diffraction peak at 2θ = 26.5 deg, which one does not belong to the $CuInS_2$ (See 3.1.2. Figs. 3.4 and 3.5). Obviously, $CuIn_5S_8$ present in the films sprayed at Cu/In≤ 1 upon annealing transforms into $CuInS_2$ and In_2S_3, whereby In_2S_3 evaporates during the annealing. A similar conclusion was made for the Cu-poor CIS films prepared by ALD and heat treated in the H_2S atmosphere at 500 °C [91].

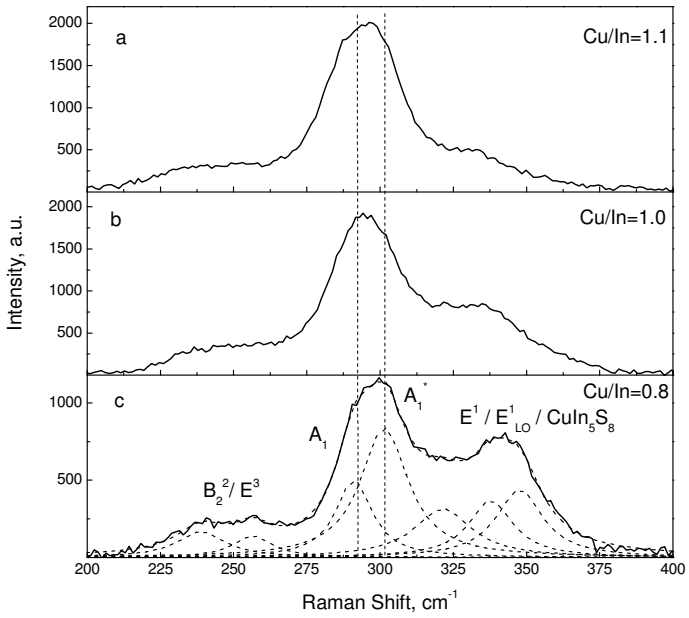

Fig. 3.7. Raman spectra of as-deposited $CuInS_2$ films at Cu/In= 1.1 (a), Cu/In= 1.0 (b), Cu/In= 0.8 (c) in solution. Fitting results are shown with a dash line (c).

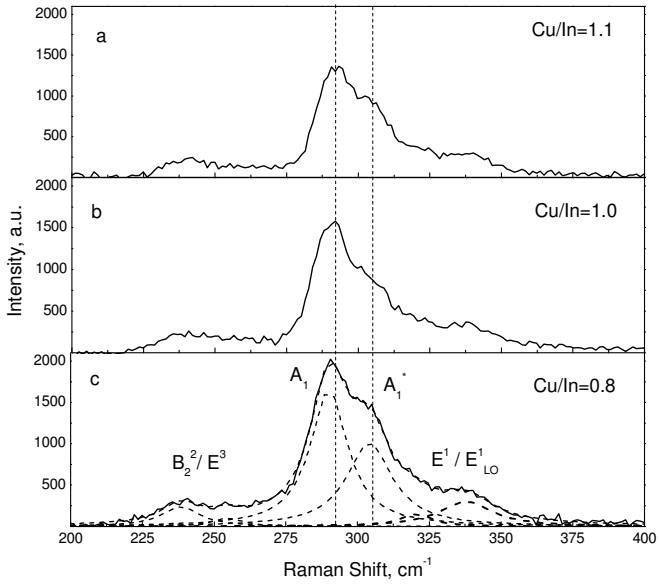

Fig. 3.8. Raman spectra of $CuInS_2$ films heat-treated in H_2S at 525 °C: Cu/In= 1.1 (a), Cu/In= 1.0 (b), Cu/In= 0.8 (c) in solution. Fitting results are shown with a dash line (c).

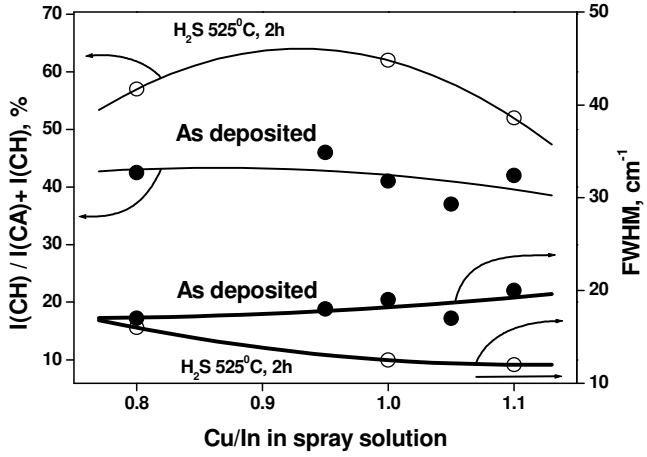

Fig. 3.9. Quality factor describing the chalcopyrite structure ratio for the Cu-Au ordering structure of $CuInS_2$ as deposited and annealed at 525^0C in the H_2S atmosphere and FWHM of the A_1 band of the $CuInS_2$ as deposited and and annealed at 525^0C in the H_2S atmosphere.

A_1 mode intensity ratio into the total intensities of A_1 and A_1^* modes (I(CH)/ I(CH)+I(CA)) has been used to characterise the material quality (Fig. 3.9). This ratio is between 40-45% for as-deposited films. Heat treatment in the H_2S environment at 525 °C increases the volume of CH up to 62 %. The FWHM (full width half maximum) of A_1 Raman band (CH structure) decreases from 18-20 cm^{-1} down to 12-13 cm^{-1} (Fig. 3.9). The increase in the intensity of A_1 chalcopyrite Raman band as compared to A_1^* mode of Cu-Au ordered structure together with the narrowing of the FWHM of the main CH Raman band shows that post-deposition thermal treatment in the hydrogen sulfide atmosphere at the temperatures above 500 C could be used to improve the structural quality of $CuInS_2$ films prepared by spray pyrolysis technique. However, by the treatment used in this work the CIS film still contains both, chalcopyrite and unwanted Cu-Au ordered $CuInS_2$. Thus, further investigations are needed to elaborate on the conditions to obtain the films containing chalcopyrite $CuInS_2$.

3.2. Optical properties of spray deposited and annealed CIS films

3.2.1. Optical properties of as-sprayed CIS films

The results covering the optical properties of as-sprayed CIS films are presented in [II, VII].

Optical transmittances of spray deposited CIS films with similar thicknesses strongly depend on the precursors' molar ratio in the solution (Fig. 3.10). The increase in the copper concentration in the spray solution reduces film transmittance.

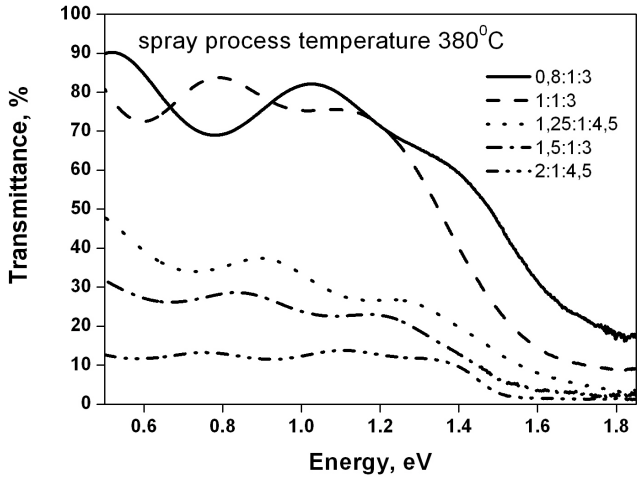

Fig. 3.10. Optical transmittance spectra of sprayed $CuInS_2$ prepared at 380^{0}C using different Cu/In molar ratio in solution.

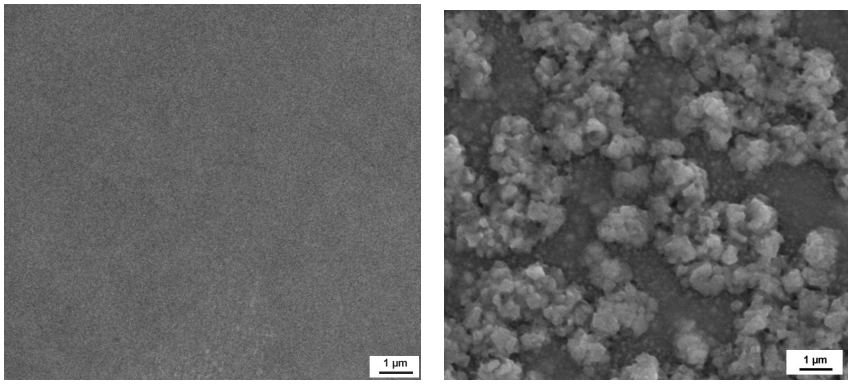

a) b)

Fig. 3.11. SEM micrograph of $CuInS_2$ films prepared by spraying the In-rich solutions (a) and the Cu-rich solutions at substrate temperature 380^0C.

The behaviour observed could be explained by the drastic changes in the surface morphology depending on the Cu/In in the spray solution [I, V]. According to the SEM study, the films from In-rich solutions, similarly to those prepared from the solutions with the Cu/In=1 and 1.1, show a smooth surface (Fig. 3.11. a). The surface becomes rough if the copper content in the spray solution is increased (Cu/In > 1.25) (Fig. 3.11. b). The films consist of two different areas – the flat area and the domains with large grains (Fig.3.11.b). Thus, the decreased optical transmittance of the films deposited from "Cu-rich" solution in the spectrum region $h\nu$<1.5 eV is mostly due to the light scattering from the rough surface. The mechanism of the formation of large grain domains has thoroughly discussed by O. Kijatkina [64]. In addition, highly irregular surface morphology together with different elemental composition in the flat area and large grain domains [V] can make the films irrelevant for the devices.

The absorption coefficient α was calculated using the expression (3.2)

$$\alpha = \frac{1}{d}\ln\frac{I_0}{I}, \quad \text{where} \qquad (3.2)$$

d is the thickness of the film acquired from SEM cross-section images of the film, I_0 is the intensity of the incident radiation, *I* is the intensity of the transmitted radiation. The absorption coefficient was calculated for the films which did not show a very rough surface (Cu/In ≤ 1.25 in the solution). Scattering and reflection of the initial radiation was not taken into account as the measurement system does not allow us to record the reflectance spectra.

The absorption coefficient α in the spectral region below the absorption edge (hν>1.5 eV) was found to be ≥ 10^4 1/cm for the sprayed CIS films, whereas the deposition temperature (320^0C or 380^0C) has an insignificant effect.

The optical bandgap of as-sprayed and thermally treated films was deduced from the transmittance or absorbance spectra measured at room temperature. Following

the conventional analysis, the energy dependent absorption coefficient can be expressed by the relation (Eq 3.3) for the allowed direct transition as

$$\alpha \cdot h \cdot \nu = A(h \cdot \nu - E_g)^{\frac{1}{2}}, \text{ where} \quad (3.3)$$

A is a parameter depending on the transition probability, E_g a direct band gap, α - absorption coefficient, h - Planck's coefficient, ν - frequency of the radiation.
Thus, E_g was found from the plot $(\alpha \cdot h \cdot \nu)^2$ versus the photon energy $h \cdot \nu$ by extrapolating the linear portion of the plot up to α=0 as shown in Fig. 3.12.

Table 3.2. Film thickness d, transmittance T at λ=1000 nm, optical bandgap E_g and morphology of sprayed films depend on growth temperature and Cu/In ratio in solution

t_s, °C	Cu/In	d, μm	Surface	T, %	E_G, eV
320	0.8	0.6	smooth	70	1.45
	1.0	0.6	≈smooth	70	1.42
	1.25	≈0.6	rough	45	1.40
380	0.8	0.5	smooth	70	1.44
	1.0	0.5	≈smooth	70	1.41
	1.25	≈0.6	rough	25	1.40

The numerical data of transmittance at λ=1000 nm and E_g of CIS films deposited at temperatures of 320^0C and 380^0C using different solution composition are presented in the Table 3.2. As-sprayed CIS films show the optical band energy gap of 1.40-1.45 eV [II, VII], corresponding to the literature data for spray-deposited $CuInS_2$ films [54, 62], as well as for those prepared by reactive annealing [100] or sulfurisation of Cu-In alloys [97].
The optical bandgap values lower than 1.5 eV could be explained by the existance of other phases in sprayed films that have the bandgap smaller than $CuInS_2$, for example, $CuIn_5S_8$ has E_g=1.4eV at 300 K [101]. Moreover bandgap tailoring disturbs optical bandgap calculations.

3.2.2. Optical properties of H_2S treated CIS films

Optical properties of CIS films annealed in the H_2S atmosphere are presented in the paper [VII]. Band gap value was found to depend on the annealing temperature, treatment time and cooling conditions. H_2S treatment at 450 and 530 °C for two hours followed by rapid cooling resulted in the bandgap value of 1.45 and 1.48 eV, respectively. Treatment in flowing H_2S at 530 °C followed by slow cooling was found to increase the band gap energy up to 1.49 eV, which is the highest value

reported for the spray deposited $CuInS_2$ films [VII]. The effect of the cooling rate on the band gap value is presented in Fig. 3.12.

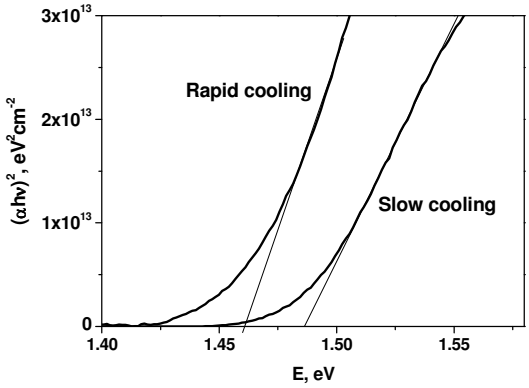

Fig. 3.12. The plot of $(\alpha h\nu)^2$ vs energy for $CuInS_2$ films deposited from "Cu-rich" solution (Cu/In=1.1) and treated for 60 minutes at 530 °C in the flowing H_2S atmosphere, subjected to rapid or slow cooling.

The widening of the optical band gap of CIS films by annealing in the H_2S atmosphere at temperatures higher than 500 °C could be explained by the improved crystallinity, by the accomplished elemental composition corresponding to $CuInS_2$ and films higher purity.
The development of film crystallinity, crystal quality (see section 3.1) and optical properties upon H_2S annealing is also supported by the changes in the elemental composition of the films, as recorded by EDX (see section 3.1.2).

3.3. Electrical properties of sprayed CIS films as-deposited and annealed in the H_2S atmosphere

The electrical properties of sprayed CIS films as-deposited and annealed in the H_2S atmosphere are presented in the publications [II, III, IV, VII].
The films were characterised by the specific resistivity, carrier type, concentration, and the activation energy of conduction mechanism. According to the hot probe measurements all sprayed films deposited at the Cu/In=0.8-4.0 in the spray solution as well the films annealed in the H_2S atmosphere show p-type conductivity and thus holes are the main carriers in all the films under study.

3.3.1. Specific resistivity of sprayed CIS films

The resistivity of the deposited films provides information about the CIS layer resistance which is part of the series resistance of the device (solar cell). The

sprayed CIS absorber layer is not homogeneous as we can see from the resistances measured by two routes – across the film (perpendicular specific resistivity) and along the surface (longitudinal specific resistivity).
The inhomogeneity of the resistivity of the sprayed CIS films is shown in Fig. 3.13. It implies that the top layer of the CIS is more conductive than the bulk and obviously the sprayed film is inhomogeneous. The difference observed could be explained by differences in the elemental composition of the surface and bulk of the film, as shown in the [64, 65]. Thus, the longitudinal resistivity of the sprayed CIS film gives misleading data for solar cell applications. In our investigations the CIS films were characterised by the resistivity measured across the film, directly reflected in the solar cell resistance.

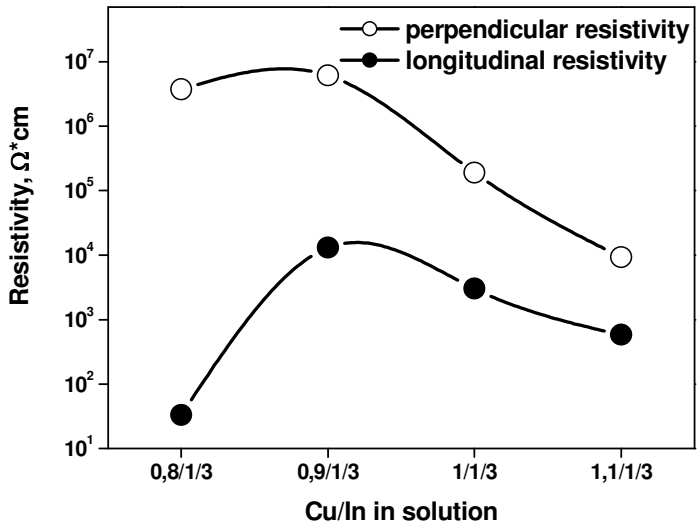

Fig. 3.13. Resistivity of the CIS film measured by two routes. Perpendicular resistivity – the current flows across the CIS film. Longitudinal resistivity – the current flows longitudinally on the CIS film surface.

The resistivities of the films with similar thicknesses deposited at different Cu/In in the solution were compared. It was found that the resistivity of the film prepared from the In-rich solution (Cu/In=0.9) is about 100 times higher than the resistivity of the film from the solution with Cu/In=1.1 (Fig. 3.13). The increase of Cu/In in the solution decreases the resistivity and could be explained by the increased crystallite size in the film using a higher copper content in the spray solution [73].
In the following experiments, Cu/In=1.0 and Cu/In=1.1 in the spray solution were used to prepare the films and study their electrical properties [VII].
The resistivities of about 10^4 Ω·cm were measured at room temperature for as-deposited CIS films at the Cu/In of 1.0 and 1.1 in the spray solution (Table 3.3)

[VII]. Similar resistivity values were reported for $CuInS_2$ films prepared by reactive sputtering [102].

Table 3.3.
Specific resistivity (ρ), concentration of carriers (Np) (from CIS/Al Schottky barrier C-V measurements at 1 kHz) at RT and conductivity activation energies (from the Arrhenius plot) for as-deposited and annealed at 530 °C in the H_2S atmosphere CIS films.

Cu:In:S in Solution	Treatment time, min	Cooling rate	ρ, Ω·cm	N_p, cm^{-3}	Arrhenius plot, T >300K E_a, meV
1:1:3	-	-	$4.6 \cdot 10^4$	$4.0 \cdot 10^{16}$	170±1
	120	Rapid	$1.0 \cdot 10^7$	$2.2 \cdot 10^{14}$	520±1
	60	Slow	$6.9 \cdot 10^5$	$1.5 \cdot 10^{17}$	83 ±1
1.1:1:3	-	-	$2.5 \cdot 10^4$	$1.0 \cdot 10^{18}$	114±1
	120	Rapid	$4.0 \cdot 10^7$	$3.2 \cdot 10^{14}$	347±1
	60	Slow	$2.5 \cdot 10^5$	$2.3 \cdot 10^{17}$	160±1

H_2S treatment, which was found to improve structural and optical properties of the films, significantly decreases film conductivity and concentration of carriers (Table 3.3). The influence of different cooling rates is distinctly expressed, whereas the Cu/In in the solution has a minor effect (Table 3.3). A resistivity of 10^7 Ω·cm is characteristic of rapidly cooled films (Table 3.3). Applying slow cooling after the treatment for one hour, the increase in the conductivity and carrier density was observed (Table 3.3). The behaviour observed is similar to that described for polycrystalline $CuInS_2$ films grown by coevaporation and subjected to annealing in the sulphur atmosphere [99], where the higher conductivity of slowly cooled films was explained by the saturation of sulphur vacancies during the cool-down period.
The results of temperature dependent conductivity measurements are presented as a plot of $ln\sigma$ vs 1000/T in Fig. 3.14. We have assumed that the mobility of holes does not significantly vary within the temperature region used.

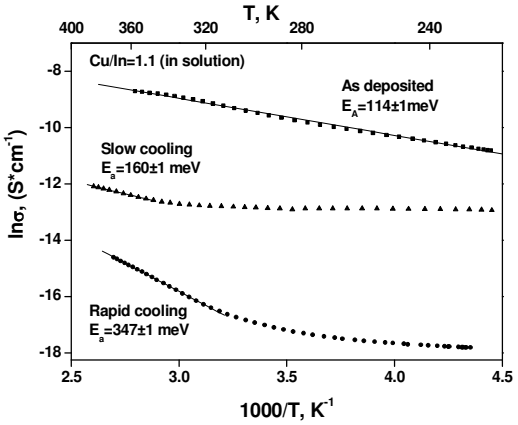

Fig. 3.14. Plot of lnσ versus 1000/T for as-deposited from Cu-rich solution (Cu/In=1.1) and annealed for 60 minutes at 530 ^{0}C in the flowing H_2S atmosphere $CuInS_2$ films subjected to rapid or slow cooling.

It could be seen that as-sprayed samples follow the thermally activated electrical conductivity σ according to the Arrhenius relation (Eq. 3.4):

$$\sigma = \sigma_0 \exp(-\frac{E_a}{kT}) \text{, where} \qquad (3.4)$$

σ_0 is pre-exponential factor, E_a is the activation energy, k is the Boltzmann's constant. The thermal activation energies 114±1 meV and 170±1 meV were obtained for as-sprayed films deposited from "Cu-rich" (Cu/In=1.1) and "stoichiometric" (Cu/In=1.0) solutions, respectively.

The plots of lnσ vs 1000/T of H_2S treated films show a parabolic behaviour (Fig. 3.14) and thus the mixed conductivity activation mechanism due to the defect levels and grain boundary effects could be proposed [17, 103]. Parabolic behaviour is highly pronounced for films subjected to rapid cooling. With the samples cooled down slowly, the increase in the conductivity with a less pronounced curvature of lnσ vs 1000/T plot was observed.

At a high temperature region (T > 320 K) the plot of lnσ vs 1000/T of H_2S treated films follows the Arrhenius dependence for both, rapidly and slowly cooled samples. Infinitely high activation energies of 340±1 and 520±1 meV were found for rapidly cooled samples prepared from "Cu-rich" and "stoichiometric" solutions, respectively (Table 3.3). We believe that these activation energies indicate that there are residues of some unknown phase between the grains in rapidly cooled samples and are not caused by some very deep acceptor level in $CuInS_2$. An indium and sulphur containing phase was detected on the surface of the film from a

"stoichiometric" solution after rapid cooling as shown in [VII]. A similar phase could be present at grain boundaries as well. The presence of an indium sulphide phase at grain boundaries has been reported for sprayed CIS films annealed in the sulphur atmosphere [74].
By slow cooling, this highly resistive phase disappears and the conductivity of samples increases. Thus, the slow cooling results in thermal activation energies of the conductivity of 80 and 160 meV (for the samples grown from "stoichiometric" and "Cu-rich" solutions, respectively), which could be assigned to acceptor levels in $CuInS_2$.

3.3.2. Concentration of carriers in sprayed as-deposited and H_2S annealed CIS films

Concentration of carriers was determined from C-V measurements of $CuInS_2$/Al Schottky barriers and ZnO/CdS/$CuInS_2$ solar cell structures. The results are published in [III, VII].
The solar cell structure, as the final goal of the CIS film application, is also part of the material investigations. The solar cell structure, consisting of the CIS absorber layer, buffer layer and window layer, could be investigated by applying the Schottky barrier model. Assuming the depletion layer of the solar cell inside the CIS layer and the window layer as the metal like electrode, one can measure the carrier concentration exactly in the working region of the CIS layer. The region between the buffer layer and absorber the layer is the region of the interface states. Therefore, the Schottky barrier model is disturbed and the results on carrier concentrations are rough.
C-V curves of $CuInS_2$/Al Schottky barriers and ZnO/CdS/$CuInS_2$ solar cell structures were recorded in the region of voltages from –2 V up to 0.5 V at 1 kHz [III, VII]. The carrier concentrations in CIS calculated from the slope of $1/C^2$ versus voltage plot of the CIS/Al Schottky barrier are presented in Tables 3.3. and 3.4, as determined from the solar cell structure. The carrier concentrations in the sprayed CIS layer are on the level of $\sim 1 \cdot 10^{17}$ cm^{-3}, as calculated from the p-n junction in a superstrate configuration solar cell. In this case, the Cu/In molar ratio in the solution has no considerable effect on the concentration of carriers [III]. The concentration of carriers in as-deposited films determined from the CIS/Al Schottky barrier (Table 3.3) at the CIS preparation from the solution with the Cu/In=1 is close to that determined from the p-n junction and reported in literature [104] The use of the Cu/In =1.1 results in carriers concentration close to $\sim 1 \cdot 10^{18}$ cm^{-3} [VII]. The differencies in the concentrations of carriers from the Schottky barrier and solar cell could also be explained by the sprayed films inhomogeneity (in surface and back).

Table 3.4.
Carrier concentrations in $CuInS_2$ films as determined by C-V measurements of sprayed $ZnO/CdS/CuInS_2$ solar cells and output characteristics of sprayed $ZnO/CdS/CuInS_2$ solar cells

Cu/In molar ratio in solution	Solar cell			
	V_{OC}, mV	j_{SC}, mA/cm^{-2}	FF	N_p, cm^{-3}
0.9	336	0.26	0.27	$1.8 \cdot 10^{17}$
1.0	443	5.5	0.37	$2.1 \cdot 10^{17}$
1.1	380	3.4	0.38	$8.7 \cdot 10^{16}$

The H_2S treatment was found to decrease the specific conductivity by three orders and a similar decrease was observed in the concentration of carriers. The concentration of carriers in the order of 10^{14} cm^{-3} is characteristic of rapidly cooled films (Table 3.3). Such low carrier concentration is reported for $CuInS_2$ films prepared by the sulphurisation of stacked Cu-In layers [54] and reactive sputtering in H_2S [105] as well as for as-grown single crystals [56]. It is believed that such a low carrier density is a sign of heavy compensation since the concentration of intrinsic defects in this material is reported to be much higher [56]. Applying slow cooling after the treatment for one hour, an increase in carrier density up to ~$1 \cdot 10^{17}$ cm^{-3} was observed (Table 3.3). Similar behaviour is reported for polycrystalline $CuInS_2$ films grown by coevaporation and subjected to annealing in sulphur atmosphere [84]. The conductivity of slowly cooled films is still lower than that of as-prepared films. The temperature dependent conductivity measurements indicate that the effect of the grain boundaries should be considered in the conductivity mechanism (Fig. 3.14). To solve the problem of low conductivity, further studies involving the mobility measurements are needed.

3.4. Solar cell structures based on as-sprayed CIS absorber layer

Superstrate configuration solar cell structures (wide band gap window layer of ZnO or TiO_2, buffer layer of CdS or In-O-S and absorber layer of $CuInS_2$) were prepared either entirely by spray pyrolysis or in combination with the CBD technique. The principal scheme of the superstrate conguration solar cell is presented in Fig. 3.15. Results are published in [III, IV].

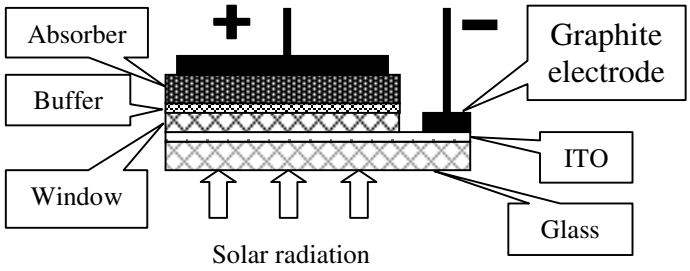

Fig. 3.15. The superstrate solar cell configuration under the observation in this work.

The specialities of spray pyrolysis process precursors as the most suitable deposition temperature of ZnO [106], TiO_2 [107], In_2S_3 [108] and CIS [64], are supporting the use of superstrate configuration design for all layers sprayed solar cells. In this case, the window layer is prepared at the highest temperature and the next ones (buffer and CIS) at lower temperatures without disconnecting the deposition process, except to adjust the temperature. There is an additional benefit, as only one glass is needed in this case [109]. ZnO and TiO_2 were prepared as described in [110, 107]. The deposition of buffer layers is described in [III, IV].
Solar cells were characterized by I-V curves in dark and under the illumination of 100 mW/cm^2, diode ideality factor n, output characteristics (*jsc,* V_{oc}, *FF*, efficiency), junction barrier height Φ_b, and the temperature dependent frequency swept admittance spectroscopy. So far, the electrical characterisations are performed on high quality solar cells prepared by vacuum-based technologies and only few on solar cells prepared by low cost techniques [91, 111].

3.4.1. Effect of preparation conditions of the CIS absorber layer on solar cell characteristics

Solar cell performance depends on many variables, each of which needs an adjustment to the optimal value. The properties of sprayed $CuInS_2$ absorber layer, the most important part of the solar cell, are mainly controlled by Cu/In molar ratio in the spray solution [64]. Thus, a set of all layers sprayed ZnO/CdS/CuInS2 solar cells were prepared using different spray solution composition (Cu/In in solution) to deposit the absorber layer, keeping other deposition parameters and underlayers invariable.

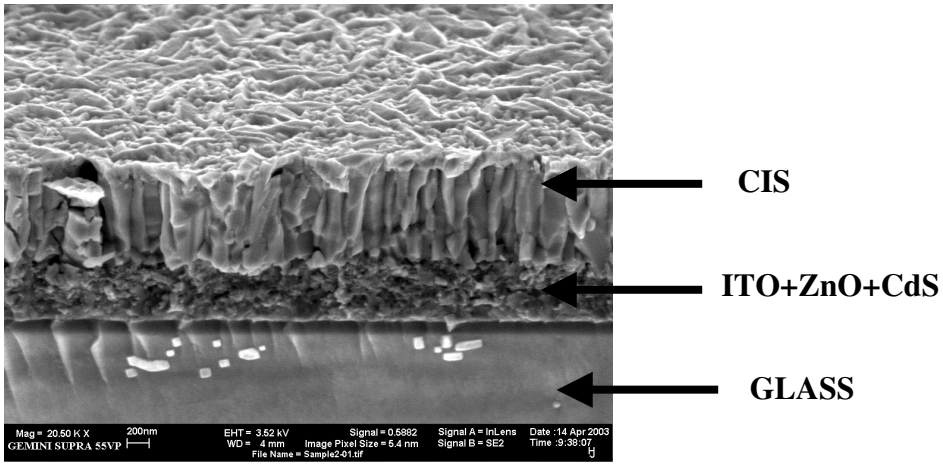

Fig. 3.16. SEM micrograph of all-layers-sprayed solar cell cross-section.

The SEM cross-sectional micrograph of all layers sprayed ZnO/CdS/$CuInS_2$ cell is presented in Fig. 3.16. Characteristic I-V curve of all layers sprayed ZnO/CdS/$CuInS_2$ cell based on CIS prepared with the Cu/In=1 in solution is shown in Fig. 3.17 and the graph for the calculation of diode ideality factor in Fig. 3.18. The cell output characteristics depending on the Cu/In in solution are presented in Table 3.5.

Solar cells based on the CIS absorber prepared from slightly In-rich (Cu/In=0.9) and stoichiometric (Cu/In=1.0) solutions exhibit the open circuit voltages of 417 mV and 443 mV, respectively, short circuit current densities between 5-6 mA/cm^2, the fill factor around 40%, resulting in a conversion efficiency of 1% at RT. The increase in copper concentration in the spray solution decreases the open circuit voltage and the efficiency of the cell (Table 3.5).

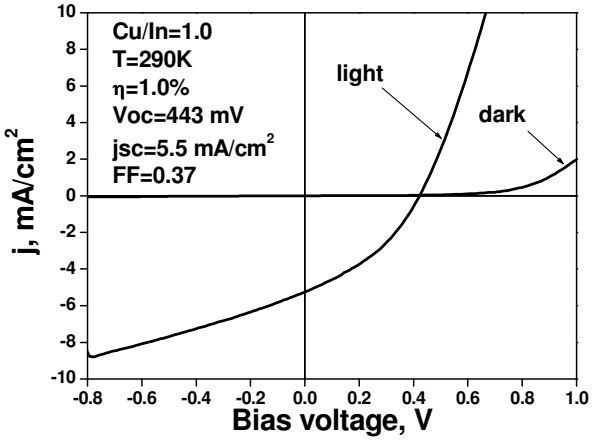

Fig. 3.17. Current-voltage characteristic of the ZnO/CdS/CIS all layers sprayed solar cell in dark and under the illumination of 100 mW/cm^2.

The diode idealiy factor of about 4 was calculated for the best cell (Fig. 3.18), which is much higher than reported for the solar cells with the efficiency around 10 % [113]. The deposition of the absorber from In-rich or Cu-rich solutions results in higher diode ideality factors. Thus, a high diode ideality factor indicates that the dominating recombination path could be caused by the interface states [83].

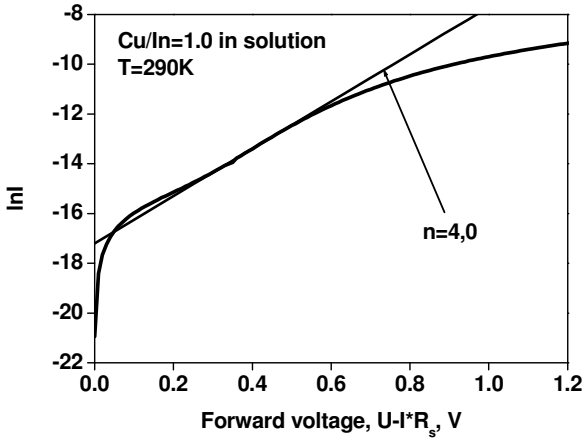

Fig. 3.18. I-V curve of the ZnO/CdS/CIS all layers sprayed solar cell based on CIS absorber deposited at the Cu/In=1.0 in solution. The ideality factor was calculated from the the presented slope.

Table 3.5.
Parameters of ZnO/CdS/CIS all layers sprayed solar cells based on CIS absorber layers prepared at different Cu/In molar ratio in spray solution

Cu/In in solution	j, mA/cm^2	V_{oc}, mV	FF, %	η, %
0.9	5.7	417	44	1
1.0	5.5	443	37	1
1.1	5.8	379	41	0.9
1.25	4.5	390	44	0.8
1.5	4.8	282	46	0.5

The temperature dependent open circuit voltage (V_{oc}) measurements were performed, where the open circuit voltage at 0 K ($V_{oc}(0)$) determines the barrier height of p-n junction Φ_b as shown in Fig. 3.19. It could be seen that the barrier height is definitely lower than the bandgap energy of sprayed CIS (E_g=1.45 eV). This is an evidence of the interface recombination as the main recombination path for the photogenerated electrons [112]. Barrier heights of the p-n junction depending on the absorber layer preparation conditions (Cu/In in spray solution) are shown in Fig. 3.20.

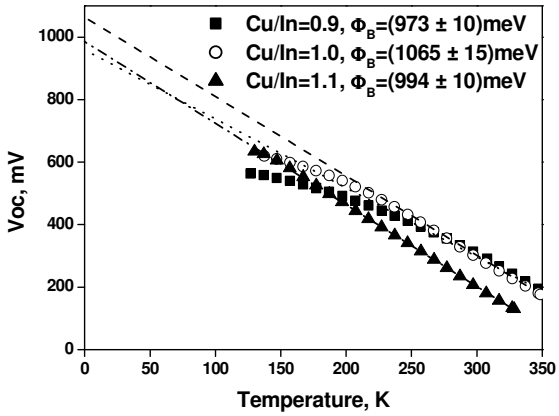

Fig. 3.19. Open circuit voltage of the solar cells versus temperature. Corresponding barrier heights for the cells with different aborbers are presented.

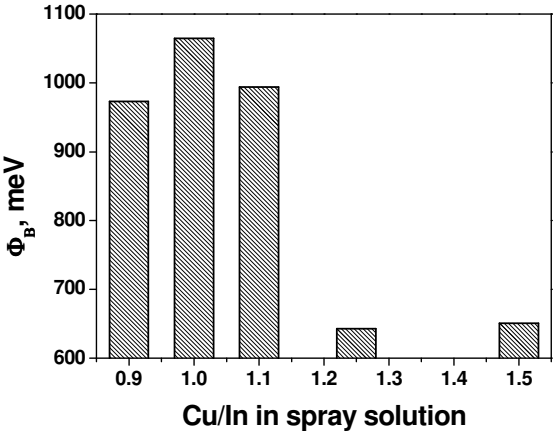

Fig.3.20. P-n junction barrier height in solar cells, depending on the Cu/In ratio in the absorber layer spray solution.

The temperature dependent frequency swept admittance spectroscopy was applied to determine the activation energy (E_A) of the dominant energy dissipation channel. The typical capacity versus the frequency plot of the ZnO/CdS/CIS structure (CIS deposited at Cu/In=1) is shown in Fig. 3.21. The frequency of the inflection point (f_i) depends on the temperature according to the Arrhenius law. The activation energy (E_A) of the recombination levels is determined from the slope of the plot $ln(\omega_i/T^2)$ vs $1/T$, where ω_i is the angular frequency of the inflection point (See Fig. 3.21) [115]. The determination of the activation energies is shown in Fig. 3.25. (see section 3.4.2).

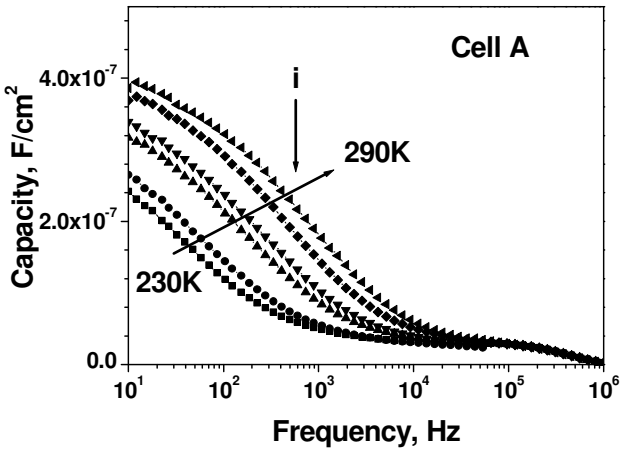

Fig. 3.21. Capacity versus frequency measured at various temperatures for the ZnO/CdS/CIS cell. (*i* is the inflection point).

The frequency-swept admittance measurements were performed at DC biases from –2V up to + 0.5V. The complex impedance plot of Z" versus Z' (not presented) shows one semicircle, indicating the presence of a single barrier. The frequency of the maxima of $tan\delta$ ($tan\ \delta = Z''/Z'$, where Z'' is a imaginary part and Z' is a real part of the impedance) was found to depend on the applied bias for the ZnO/CdS/CIS cell, as shown in Fig. 3.22. If the junction frequency dependent capacitance (or conductance) or some other characteristic derived from these parametres is found to depend on the voltage applied to the p-n junction, one can assume that a lowered barrier height is caused by the interface states [114, 115]. The observed behaviour confirms that the calculated activation energy E_A should be attributed to the dominant interface states at the interface of the p-n junction [103].

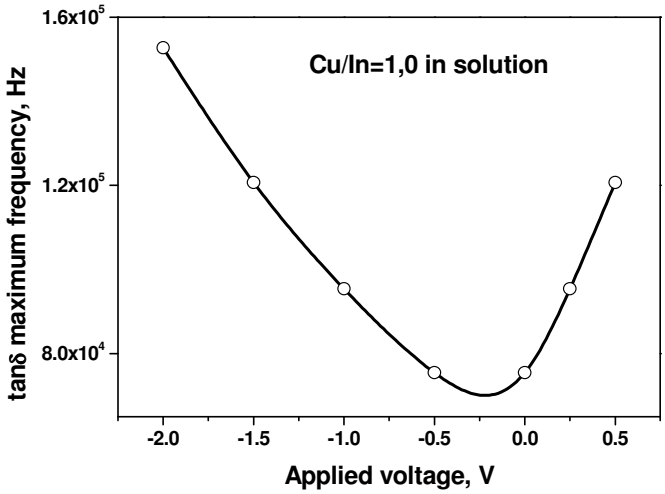

Fig. 3.22. Frequency of the *tanδ* maxima of complex impedance plots (*Z"* vs *Z'*) vs applied bias.

In conlusion, the recombination at the p-n junction interface is the limiting factor of the solar cell open circuit voltage, as shown by the ideality factor of the cell I-V curves and barrier height measurements, and in addition, confirmed by the admittance measurements at different DC biases. The use of Cu-rich solutions to the deposit CIS absorber layer, which allows to grow the absorber with larger crystallities, significantly reduces the p-n junction barrier height and the cell open circuit voltage.

3.4.2. Effect of buffer layer type and preparation technique on solar cell characteristics

Attempts have been made to modify the sprayed CIS based solar cell by the buffer layer type and deposition techniques. In addition to the spray, the CdS buffer layer was deposited by chemical bath deposition (CBD) method. Also, In sulphide based buffers were deposited by spray and CBD. All the other layers (window and absorber) and their deposition parametres by spray remained constant. CIS absorber was deposited using the Cu/In=1 in spray solution (see section 3.4.1). Our goal was to test the effect of different buffers on the interface recombination and cell output parametres. The parameters of the cells are summarised in Table 3.6.

Table 3.6.
Parametres of superstrate configuration solar cells based on the sprayed CIS absorber layer and different buffer layers

cell	buffer	j, mA/cm^2	V_{oc}, mV	FF, %	η, %	Φ_b, meV	E_A, meV
A	CdS spray	6.7	443	37	1.0	1060±10	308±20
B	In-O-S spray	4.3	397	36	0.60	1057±10	417±20
C	In-O-S CBD	14.6	456	43	2.9	1254±10	200±10
D	CdS CBD	2.3	456	37	0.4	1185±10	260±10

The CBD technique used in In_2S_3 buffer layer preparation has led to a significant advancement of the efficiency of the solar cell. The I-V curve of the cell C (CIS absorber was prepared by spray onto the CBD deposited In-sulphide buffer layer) is presented in Fig. 3.23. The diode ideality factor is 2.7, which is lower than that for a cell with a sprayed CdS buffer layer (See Fig. 3.18). The cell output parametres of open circuit voltage of 456 mV, short circuit current density of 14.6 mA/cm^2 and fill factor of 43 % result in an efficiency of 2.9 %. Although cell output parametres are still far from that reported for the best cells based on $CuInS_2$ prepared by more developed vacuum-based methods, it is shown that the working cell could be prepared in combination with low cost methods.

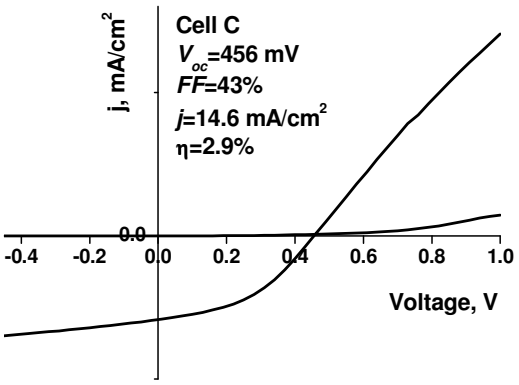

Fig. 3.23. Current-voltage characteristic of the ZnO/In-O-S/CIS a solar cell in dark and under the illumination of 100 mW/cm^2.

As that kind cells could be prepared almost within 30 minutes, their net cost is very low. It is likely that the properties could be significantly improved during the ongoing researh work. Then the patent application has been submitted [VIII].
All the investigated cells, independent of the buffer layer material and deposition technique, showed the junction barrier heights lower than the absorber layer bandgap energy of 1.45 eV (Table 3.6), indicating the main recombination path via the interface states (see section 3.4.1). The change of the sprayed CdS buffer layer by the sprayed In_2S_3 buffer layer did not change the barrier height, but increases the activation energy of the dominant interface recombination centres (cell B). Buffer layer preparation by the CBD technique increases the barrier height. The highest barrier height of 1254 meV was obtained for cell C with a In-O-S buffer layer prepared by CBD (Fig. 3.24).
The activation energies of the recombination level were calculated from the the slope of the plot $ln(\omega_t/T^2)$ vs $1/T$ (ω_t is the angular frequency of the inflection point) presented in Fig. 3.25.

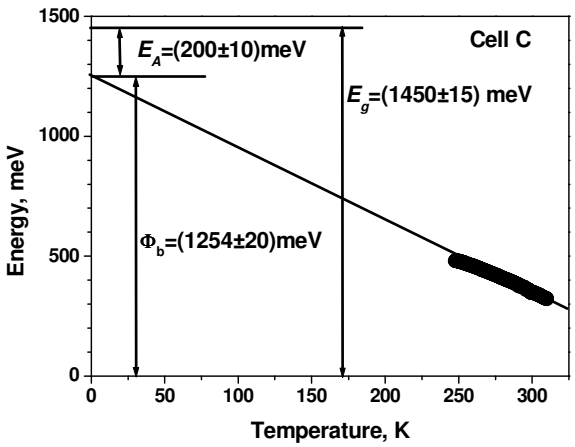

Fig. 3.24. Bandgap and barrier height (determined from the V_{oc} vs temperature measurements) of cell C (In-OH-S buffer by CBD).

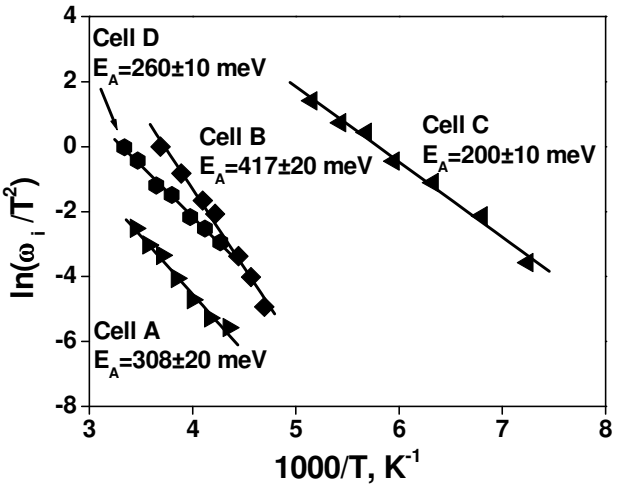

Fig. 3.25. Plot $ln\ (\omega_i/T^2)$ vs $1/T$ (ω_i is the angular frequency of the inflection point).

The results of our study show that buffer layers by chemical bath deposition technique are more suitable in combination sprayed CIS absorber layer as the decrease in the interface states energy level and increase in p-n junction barrier height has been recorded resulting in a higher open circuit voltages compare to the cells with sprayed buffer layers.

Conclusions

1. The phase composition of copper indium disulphide films prepared by spray pyrolysis, depend on the Cu/In molar ratio in the spray solution. The use of In-rich solutions results in $CuInS_2$ films containing a secondary phase of $CuIn_5S_8$. As-deposited $CuInS_2$ contains both, chalcopyrite and Cu-Au ordered domains of $CuInS_2$, independent of the Cu/In molar ratio in the spray solution.

2. The crystallite size of as-deposited films is controlled by the Cu/In molar ratio in an the spray solution. The spraying of In-rich solutions results in $CuInS_2$ films with crystallite size in order of 10 nm, whereas the spray of Cu-rich solutions result in the (112) orientated $CuInS_2$ films with the crystallite size up to 120 nm.

3. Post-deposition treatment at 525 °C in the H_2S atmosphere yields in $CuInS_2$ films with closely stoichiometric composition, with the crystallite size of 300 nm and optical bandgap of 1.49 eV independent of the Cu/In molar ratio used to deposit the films. H_2S treatment increases the amount of $CuInS_2$ chalcopyrite structure up to 62% and decreases the FWHM of chalcopyrite main Raman peaks down to 12 cm^{-1}, showing improvement in the crystal quality of the films.

4. As-deposited $CuInS_2$ films show p-type conductivity with carriers concentration around $1*10^{17}$ cm^{-3} and the specific resistivity of 10^4-10^5 Ω·cm using Cu/In=0.9–1.1 in the spray solution. H_2S treatment significantly decreases film conductivity and the concentration of carriers, whereas the cooling down rate has a considerable effect. Rapid cooling results in highly resistive films with a specific resistivity around ~$1\cdot10^7$ Ω·cm and carriers concentration in order of ~$3\cdot10^{14}$ cm^{-3}, slow cooling down decreases the resistivity to ~$1\cdot10^5$ Ω·cm and increases the carrier concentration up to ~$1\cdot10^{17}$ cm^{-3}. Parabolic behaviour of the plots $ln\sigma$ vs $1/T$ of H_2S treated films refers to the mixed conductivity activation mechanism due to the defect levels and grain boundary effects.

5. The working capacity of the sprayed $CuInS_2$ layer as a solar cell absorber was tested in superstrate configuration $ZnO/CdS(In_xS_y)/CuInS_2$ cells prepared entirely by spray pyrolysis or in combination with the chemical bath deposition (CBD) technique. The interface recombination path and high series resistance are assumed to be the main limiting factors of the cell efficiencies.

6. In an all-layers-sprayed cell the highest efficiency of 1.0 % is achieved using Cu/In =1.0 to deposit the $CuInS_2$ absorber layer. The use of Cu-rich solutions to deposit the absorber layer decreases the p-n junction barrier height and the efficiency of the cell. The use of CBD technique to deposit the In-O-S buffer layer instead of sprayed CdS increases the barrier height from 1060 meV to 1250 meV and results in the conversion efficiency of 2.9 % with V_{oc}=456 mV, j_{SC} =14.6 mA/cm^2 and FF=43 % at the illumination of 100 mW/cm^2.

Acknowledgements

This thesis is based on the experimental work carried out at the Department of Materials Science, Tallinn University of Technology.

I wish to express my deep gratitude to my supervisor, Prof. Malle Krunks, for her support, encouragement and advice during this work.

I would like to thank my colleagues and coauthors Dr. Olga Kijatkina, MSc Ilona Oja, Dr. Valdek Mikli, MSc Atanas Katerski for their contributions, and Prof. Jyri Krustok for useful discussions.

I am also very grateful for the help, present and past, by Prof. Enn Mellikov, Prof. Urve Kallavus, members of the Centre for Materials Research, Departments of Materials Science and Physics.

The Estonian Ministry of Education and Research, the Estonian Science Foundation (grants 4270, 5612) and the European Commission (project HRPN-CT-2000-00141) are acknowledged for the financial support.

My warmest thanks belong to my family.

Tallinn, January 2006

Abstract

Structural and Electrical Properties of Spray Deposited Copper Indium Disulphide Films for Solar Cells

$CuInS_2$ (CIS) is one of the most promising absorber materials for thin film solar cells due to its bandgap of 1.5 eV, high absorption ability and high theoretical efficiency of 28.5%. CIS is non-toxic. Polycrystalline thin film could be deposited by different methods. A key factor in reducing of the cost of PV modules is connected with the manufactoring processes. Thus, during last years the interest was also directed to development of low cost wet chemical techniques including spray pyrolysis, which is a convienent and rapid method to deposit large area films. Due to low efficiency of 1-2% of sprayed CIS absorber layer based solar cells, the spray deposited CIS is poorly investigated.

This work is dedicated to the complex of studies of structural and electrical properties of spray deposited CIS films as an absorber layer for solar cell. The objectives of the doctoral thesis were to study:

– the phase composition and crystallinity of spray-deposited CIS films depending on the Cu/In molar ratio in the solution;

– the effect of annealing in the hydrogen sulphide atmosphere on the phase composition, crystallinity and optical properties of sprayed CIS films;

– electrical parameters, such as conductivity and carriers' concentration in as-deposited and annealed in hydrogen sulphide atmosphere CIS films;

– the effect of the Cu/In molar ratio in the CIS spray solution and the buffer layer type on solar cell solar cells parameters.

The doctoral thesis is based on 7 published papers. As a result of studies, a provisional US patent application is on hand. The main results are as follows:

The use of In-rich solutions results in $CuInS_2$ films containing a secondary phase of $CuIn_5S_8$. As-deposited $CuInS_2$ contains both, chalcopyrite and Cu-Au ordered domains of $CuInS_2$ independent of the Cu/In molar ratio in the spray solution. Crystallite size of as-deposited films is controlled by the Cu/In molar ratio in the spray solution.

Post-deposition treatment at 525 °C in the H_2S atmosphere yields in $CuInS_2$ films with closely stoichiometric composition, crystallite size of 300 nm and optical bandgap of 1.49 eV. H_2S treatment increases the amount of $CuInS_2$ chalcopyrite structure up to 62%.

As-deposited CIS films (Cu/In=0.9–1.1 in solution) show concentration of holes of $1 \cdot 10^{17}$ cm^{-3} and specific resistivity of 10^4-10^5 Ω·cm. Rapid cooling after H_2S treatment was found to be unsuitable as resulted in very high resistivity of 10^7 Ω·cm. Slow cooling down is preferred as resulting in resistivity of 10^5 Ω·cm and carriers concentration of ~10^{17} cm^{-3}.

The working capacity of sprayed CIS was tested in superstrate configuration ZnO/CdS(InxOSy)/CIS cells prepared entirely by spray pyrolysis or

in combination with CBD technique. The strong interface recombination and high series resistance obviously are the main limiting factors of the cell efficiencies. In all-layers-sprayed cell the highest efficiency of 1.0 % is achieved using the Cu/In =1.0 to deposit the CIS absorber layer. The use of Cu-rich solutions to deposit the absorber layer decreases the p-n junction barrier height. In-O-S buffer by CBD technique increases the barrier height. from 1060 meV to 1250 meV and results in conversion efficiency of 2.9 % with Voc=456 mV, j_{SC} =14.6 mA/cm^2 and FF=43 % at illumination of 100 mW/cm^2.

Kokkuvõte

Pihustussadestatud vaskindiumdisulfiidkilede struktuursed ja elektrilised omadused ning rakendus päikesepatareides

$CuInS_2$ (CIS) on sobiv absorberkihi materjal õhukesekihilistes päikesepatareides teoreetilise kasuteguriga 28,5%, keeelutsooniga 1,5 eV ja suure absorptsioonitaguriga. $CuInS_2$ on keskkonnasõbralik ja seda on võimalik kasvatada polükristallilisena mitmel meetodil. Päikesepatareide seisukohalt on saanud oluliseks toodetava energia hind, mis on seotud tootmise hinnaga. Viimasel ajal pööratakse suurt tähelepanu keemilistele vedeliksadestusmeetoditele. Nende hulgas on tähelepanuväärseim pihustuspürolüüs, mis on kiire ja sobilik meetod suurte pindade katmiseks. Pihustuspürolüüsi meetodil valmistatud õhuke $CuInS_2$-kile on väheuuritud materjal, kuna sellest valmistatud päikesepatarei kasutegurid on siiani olnud 1-2%.

Käesolev töö on pühendatud pihustuspürolüüsi meetodil valmistatud polükristalse $CuInS_2$-kile struktuursete ja elektriliste omaduste kompleksele uurimisele eesmärgiga hinnata selle materjali kasutamise võimalusi päikesepatareides.

Töös on uuritud:

– Pihustuspürolüüsil sadestatud $CuInS_2$-kilede faasikoostist ja struktuuri sõltuvalt Cu/In suhtest pihustuslahuses.

– $CuInS_2$-kilede järellõõmutamist väävelvesiniku keskkonnas, H_2S töötluse mõju kilede morfoloogilistele, optilistele ja struktuursetele omadustele.

– Sadestatud ja järeltöödeldud kilede elektrilisi omadusi (juhtivus, juhtivuse temperatuurisõltuvus, laengukandjate kontsentratsioon).

– Fotovoltmuundurid ja nende omadused pihustuspürolüüsi meetodil valmistatud $CuInS_2$ absorberkihi baasil, absorberkihi sadestusparameetrite ja erinevate puhverkihtide mõju fotovoltmuunduri omaduste kujunemisele.

Doktoritöö baseerub 7 artiklil, töö tulemusena on käitlemises 1 USA patenditaotlus.

Töö põhitulemused on järgmised:

In-rikaste lahuste korral sisaldab $CuInS_2$-kile teist faasi $CuIn_5S_8$. Äsja-sadestatud $CuInS_2$ sisaldab nii halkopüriitset kui ka Cu-Au korrastatud faaside domeene, sõltumata vase/indiumi suhtest lähtelahustes. Kristalliitide suurus on juhitav vase/indiumi suhtega lähtelahustes.

Järeltöötluse tulemusena 525 °C juures H_2S atmosfääris saadakse ligikaudu stöhhiomeetrilise koostisega $CuInS_2$-kiled kristalliitide suurusega 300 nm ja keelutsooniga 1.49 eV. H_2S töötlus suurendab $CuInS_2$ halkopüriitse faasi osakaalu 62%-ni.

Äsjasadestatud CIS-kiled (Cu/In=0.9–1.1 lahuses) evivad aukude kontsentratsiooni $1 \cdot 10^{17}$ cm^{-3} ja eritakistust 10^4-10^5 Ω·cm. Kiirjahutus pärast H_2S töötlust on sobimatu, sest suurendab vastuvõetamatult eritakistust kuni ~10^7 Ω·cm. Aeglane jahutus on eelistatud, kuna kile eritakistus on väiksem: ~10^5 Ω·cm ja laengukandjate kontsentratsioon on sobilik: ~10^{17} cm^{-3}.

Pihustatud CIS-kilede kasutamise sobilikkust testiti igakiht-sadestatud pealisehitusliku konfiguratsiooniga (ZnO/CdS(InxOSy)/CIS) päikesepatareis ja ka koos keemilise vanni meetodi kombineerimisega. Tugev vahekiht-rekombinatsioon ja kõrge jadatakistus on ilmselt peamised tegurid, mis määravad selliste päikese-patareide madalad kasutegurid. Cu/In=1.0 lahusest igakiht-sadestatud päikese-patarei suurim kasutegur oli 1,0%. Vaserikka lahuse kasutamisel saadi p-n-siirde madalad barjääri kõrgused.

Keemilise vanni meetodil valmistatud In-O-S puhverkihi korral suurenes siirde barjääri kõrgus 1060 meV-lt kuni 1250 meV-ni ja kasutegur kuni 2,9%-ni, kusjuures avatud ahela pinge oli 456 mV, lühisvoolu tihedus 14,6 mA/cm^2 ja täitetegur 43% valgustusintensiivsuse 100 mW/cm^2 juures.

References

[1] A Vision for Photovoltaic Technology. Report by the Photovoltaic Technology Research Advisory Council (PV-TRAK), Luxembourg: Office for Official Publications of the European Communities ISBN 92-894-8004-1, 2005, 41 pp.

[2] D. M. Chapin, C. S. Fuller, G. L. Pearson, *J. Appl. Phys,* 25 (1954) 676.

[3] A. Goetzberger, C. Hebling and H.-W. Schock, *Mater. Sci. Eng. Reports*, 40 (2003) 1-46.

[4] P.D. Maycock, *Refocus,* 6 (2005) 18-22.

[5] A. N. Tiwari, D. K. Pandya, K. L. Chopra, *Solar Energy Materials* 15 (1987) 121-133.

[6] L. L. Kazmerski, *J. Electron Spectroscopy and Related Phenomena,*150 (2006) 105-135.

[7] M. Burgelman, P. Nollet, *Solid State Ionics*, 176 (2005) 2171-2175.

[8] S. Siebentritt, *Thin Solid Films*, 403-404 (2002) 1-8.

[9] W. Diehl, V. Sittinger, B. Szyszka, *Surface and Coatings Technology,* 193 (2005) 329– 334.

[10] R. Scheer, R. Klenk, J. Klaer, I. Luck, *Solar Energy* 77 (2004) 777-784.

[11] M. Ch. Lux-Steiner, A. Ennaoui, Ch. -H. Fischer, A. Jäger-Waldau, J. Klaer, R. Klenk, R. Könenkamp, Th. Matthes, R. Scheer, S. Siebentritt and A. Weidinger, *Thin Solid Films*, 361-362 (2000) 533-539.

[12] A. Jasenek, T. Hahn, M. Scmidt *et al.*, *Proc. 16-th European PVSEC,* Glasgow, UK (2000) 982-985.

[13] J. Alavarez-Garcia, Doctoral thesis "Characterisation of $CuInS_2$ films for solar cell application by Raman spectroscopy", Barcelona (2002) 254 pp.

[14] I. Luck, J. Kneisel, K. Siemer, J. Bruns, R. Scheer, R. Klenk, N. Janke and D. Bräuni, *Sol. Energ. Mater. Sol. Cells* 67 (2001) 151-158.

[15] R. Klenk, J. Klaer, R. Scheer, M.Ch. Lux-Steiner, I. Luck, N. Meyer, U. Rühle, *Thin Solid Films* 480-481 (2005) 509-514.

[16] K. Siemer, J. Klaer, I. Luck, J. Bruns, R. Klenk, D. Bräunig, *Sol. En. Mat. Sol. Cells* 67 (2001) 159-166.

[17] R. Klenk, S. Bakehe, R. Kaigawa, A. Neisser, J. Reiß, M. Ch. Lux-Steiner, *Thin Solid F*ilms, 451-452 (2004) 424-429.

[18] J. J.M. Binsma, L.J. Giling and J. Bloem, *Journal of Crystal Growth* 50 (1980) 429-436.

[19] L. L. Kazmerski, S. Wagner, "Current Topics in Photovoltaics", 1, Edited by T.J. Coutts Academic Press, New York, (1985) 279 pp.

[20] T. Riedle, "Raman Spectroscopy for the analysis of thin CuInS2 films", Doctoral thesis, Technical University of Berlin (2002).

[21] H. Metzner, M. Brüssler, K. D. Husemann, H. J. Lewerenz, *Phys. Rev*. B, 44 (21) (1991) 11614-11623.

[22] M.S. Tomar, F.J. Garcia, *Thin Solid Films* 90 (1982) 419-423.

[23] D. S. Su, S. H. Wei, *Applied Physics Letters* 74 17 (1999) 2483-2485.

[24] S. H. Wei, S. B. Zhang, A. Zunger, *Phys. Rev*. B, 59: (1999) 2478-248.
[25] J. Alvarez-Carcia, E. Rudigier, N. Rega, B. Barcones, R. Scheer, A. Perez-Rodrigues, A. Romano-Rodriguez, J. R. Morante, *Thin Solid Films* 431-432 (2003) 122-125
[26] E. Rudigier, J. Alvarez-Garcia, I. Luck, J. Klaer, R. Scheer, *Journal of Physics and Chemistry of Solids* 64 (2003) 1977-198.
[27] E. Rudigier, Ch. Pietzker, M. Wimbor, I. Luck, J. Klaer, R. Scheer, B. Barcones, T. Jawhari Colin, J. Alvarez-Garcia, A. Perez-Rodriguez and A. Romano-Rodriguez, *Thin Solid Films*, 431-432 1 (2003) 110-115.
[28] J.Alvarez-Carcia, A. Perez-Rodriguez, B. Barcones, A. Romando-Rodriguez, J. R. Morante, *Appl. Phys. Lett*., 80(4) (2002) 562-564.
[29] J. Alvarez-Carcia, J. Marcos-Ruzafa, A. Perez-Rodriguez, A. Romano-Rodriguez, J. R. Morante, R. Scheer, *Thin Solid Films* 361-362 (2000) 208-212.
[30] P. Guha, D. Das, A. B. Maity, D. Ganguli, S. Chaudhuri, *Sol. En. Mat. Sol. Cells*, 80 (2003) 115-130.
[31] O. Lundberg, M. Bodegard, L. Stolt, *Thin Solid Films* 431-432 (2003) 26-30.
[32] R. Scheer, I. Luck, M. Kanis, M. Matsui, T. Watanabe, T. Yamamoto, *Thin Solid Films*, 392 (2001) 1-10.
[33] R. Scheer, M.Alt, I. Luck, H. J. Lewerentz, *Solar Energy Mat. Sol. Cells*, 49 (1997) 423-430.
[34] K.C.E. Mitchell, J. Ermer, D. Pier, Conf. Rec. 20th IEEE Photovoltaiv Spec. Conf., Las Vegas, (1988) 1384.
[35] F. H. Karg, *Techn. Digest of the International PVSEC-11,* Sapporo, Hokkaido, Japan (1999) 627-630.
[36] R. Klenk, U. Blieske, V. Dieterle, K. Ellmer, S. Fiechter, I. Hengel, A. Jäger-Waldau, T. Kampschulte, Ch. Kaufmann, J. Klaer, *Sol. En. Mat. Sol. Cells* 49 (1997) 349-356.
[37] J. Klaer, I. Luck, A. Boden, R. Klenk, I.G. Perez, R. Scheer, *Thin Solid Films* 431-432 (2003) 534-537.
[38] Y. B. He, W. Kriegseis, T. Krämer, A. Polity, M. Hardt, B. Szyszka and B. K. Meyer*, J. Phys. Chem. Solids* 64 (2003) 2075-2079.
[39] Y. Yamamoto, T. Yamaguchi, T. Tanaka, N. Tanahashi and A. Yoshida, *Sol. En. Mat. Sol. Cells* 49 (1997) 399-405.
[40] M. Winkler, J. Griesche, I. Konovalov, J. Penndorf , J. Wienke, O. Tober , Solar Energy 77 (2004) 705–716.
[41] S. Nakamura, A. Yamamoto, Solar Energy Materials & Solar Cells 75 (2003) 81–86.
[42] J. Möller, Ch. -H. Fischer, H. -J. Muffler, R. Könenkamp, I. Kaiser, C. Kelch and M. C. Lux-Steiner., *Thin Solid Films* 361-362 (2000) 113-117.
[43] K. K. Banger, J. D. Harris, J. E. Cowen and A. F. Hepp, *Thin Solid Films* 403-404 (2002) 390-395.
[44] J. D. Harris, K. K. Banger, D. A. Scheiman, M. A. Smith, M. H.-C. Jin, A. F. Hepp, *Materials Sci. Engin.* B98 (2003) 150-155.

[45] P. Raja Ram, R. Thangaraj, A.K. Sharma and O.P. Agnihotri, *Solar Cells* 14 (1985) 123-131.
[46] A.N. Tiwari, D.K. Pandya and K.L. Chopra, *Solar Cells* 22 (1987) 263-273.
[47] A.G. Fitzgerald, S.M. Potrous, *Solar Energy Materials* 22 (1991) 43-61.
[48] R.P. Vijaya Lakshmi, R. Venugopal, D. Raja Reddy and B.K. Reddy, *Solid State Communications* 82 (12) (1992) 997-1000.
[49] H. Bihri, C. Messaoudi, D. Sayah, A. Boyer, A. Mzerd and M. Abd-Lefdil, *Phys. Stat. Sol.* (a) 129 (1992) 193-200.
[50] C. Messaoudi, H. Bihri, D. Sayah, M. Cadène, M. Abd-Lefdil, *Journal of Materials Science Letter* Vol.11 (1992) 1234-36.
[51] R. Scheer, I. Luck, H. Sehnert, H.J. Lewerenze, *Sol. En. Mat. Solar Cells* 41-42 (1996) 261-270.
[52] M. Ortega-López, A. Morales-Acevedo, *Thin Solid Films* 330 (1998) 96-101.
[53] H. Bouzouita, N. Bouguila and A. Dhouib, *Renewable Energy* 17 (1999) 85-93.
[54] M.C. Zouagi, T. Ben Nasrallah, S. Marsillac, J.C. Bernède and S. Belgacem, *Thin Solid Films* 382 (2001) 39-46.
[55] J. Gonzalez-Hernandez, P.M. Gorley, P.P. Horley, O.M. Vartsabyuk, Yu.V. Vorobiev, *Thin Solid Films* 403-404 (2002) 471-475.
[56] S. Marsillac, M.C. Zouagi, J.C. Bernede, T.B. Nasrallah, and S. Belgacem, *Sol. En. Mat. Sol. Cells*, 76 (2003) 125.
[57] J.B. Mooney and S.B. Radding, *Ann. Rev. Mater. Sci.* 12 (1982) 81-101.
[58] R.R. Chamberlin, J.S. Skarman, *J. Electrochem. Soc*., 113 (1966) 86.
[59] M.Krunks, T. Leskelä, L. Niinistö, *Jpn. J. Appl. Phys*., Vol.39 Suppl.39-1 (2000) 181-186.
[60] Krunks, M., Leskela, T., Mannonen, R., & Niinisto, L. *Journal of Thermal Analysis and Calorimetry* 53(2) (1998) 355-364.
[61] Krunks, M., Leskela, T., Mutikainen, I., & Niinisto, L. (1999). *Journal of Thermal Analysis and Calorimetry*, 56(2), 479-484.
[62] Krunks, M., Bijakina, O., Varema, T., Mikli, V., & Mellikov, E. *Thin Solid Films* 338(1-2) (1999) 125-130
[63] Krunks, M., Mellikov, E., & Bijakina, O, *Physica Scripta* T69 (1997)189-192.
[64] O. Kijatkina, "Deposition of Copper Indium Disulphide Films by Chemical Spray pyrolysis", (2004), Thesis on Natural and Exact Sciencies B28, Tallinn University of Technology, 132 pages
[65] M. Krunks, O. Kijatkina, H. Rebane, I. Oja, V. Mikli, A. Mere, *Thin Solid Films* 403-404 (2002) 71-75.
[66] C.W. Bates *et al.*, *Thin Solid Films* 88 (1982) 273-283.
[67] J. Bougnot, S. Duchemin and M. Savelly, *Solar Cells* (1986) 221-236.
[68] B.J. Brown and C.W. Bates, *J. Appl. Phys.* 65 (5) (1990) 2517-19.
[69] S. Shirakata, T. Murakami, T. Kariya, S. Isomura, *Jpn. J. Appl. Phys.* 35 (1996) 191.

[70] M. Ortega-López, A. Morales-Acevedo, *Thin Solid Films* 330 (1998) 96.
[71] H. Bihri, C. Messaoudi, D. Sayah, M. Abd-Lefdil, M. Cadene, *Materials Chemistry and Physics* 34 1 (1993) 24-27
[72] Jerry D. Harris, Kulbinder K. Banger, David A. Scheiman, Mark A. Smith, Michael H. -C. Jin and Aloysius F. Hepp, *Materials Science and Engineering B*, 98 Issue 2 (2003) 150-155.
[73] M. Krunks, O. Bijakina, V. Mikli, H. Rebane, T. Varema, M. Altosaar, E. Mellikov, *Solar Cell Mater. Solar Cells* 69 (1) (2001) 93.
[74] S. Marsillac, M. C. Zouaghi, J. C. Bernède, T. Ben Nasrallah and S. Belgacem, *Sol. En. Mat. Sol. Cells,* 76 2, 1 (2003) 125-134.
[75] A. N. Tiwari, D. K. Pandya and K. L. Chopra, *Thin Solid Films*, 130, 3-4, 30 (1985) 217-230.
[76] H. Bouzouita, N. Bouguila and A. Dhouib, *Renewable Energy*, 17 (1999) 85-93.
[77] B.R. Pamplin, *Progress in Crystal Growth and Characterization 1* (1979) 395-403.
[78] S. Duchemin, V. Chen, J. C. Yoyotte, C. Llinares, J. Bougnot, M. Savelli, *Proc. 7-th Eur. Photovolt. Sol. En. Conf., Sevilla, Spain* (1986) 615-619.
[79] S. Duchemin, V. Chen, J.C. Yoyotte, J. Bougnot, M. Savelli, *Proc. 8th E.C. Photov. Sol. En. Conf.* (EUR 11780), Vol.2, pp. (1987) 1038-42.
[80] S. Duchemin, J. Bougnot, A. El Ghzizal, K. Belghit, Proc. 9th Eur. Com. Photovol. En. Conf., (1989) 476-479.
[81] K**.** Subbaramaiah and V. Sundara Raja, *Sol. En. Mat. Sol. Cells* 32 (1994) 1-6.
[82] J. Singh, 1996, "OPTOELECTRONICS: An Introduction to Materials and Devices", Singapore: McGraw-Hill
[83] S. Ashok, K. P. Pande, *Solar Cells* 14, 1 (1985) 61-81.
[84] H.J. Lewerenz, *Sol. En. Mat. Sol. Cells* 83 (2004)395–407.
[85] I. Konovalov, *Thin Solid Films* 451-452 22 (2004) 413-419.
[86] Lexi Shao, Kun-hui Chang and Huey-liang Hwang, *Materials Science in Semiconductor Processing* 6 5-6 (2003) 397-400.
[87] M. Turcu, U. Rau, *Thin Solid Films* 431-432, 1 Pages (2003) 158-162.
[88] L. Reijnen, "Gas-phase synthesis of sulfide absorbers for thin film and nanostructured solar cells, Doctoral thesis", 2003, Delft University of Technology.
[89] M. Krunks, V. Mikli, O. Bijakina, H. Rebane, A. Mere, T. Varema, E. Mellikov, *Thin Solid Films*, 361-362 (2000) 61.
[90] M.H. Jin, K.K. Banger, J.D. Harris, A.F. Hepp, 3rd *World Conf. Photovoltaic Sol. Energy Conv.*, Osaka, Japan, (2003) 2P-A8-21.
[91] M. Nanu, L. Reijnen, B. Meester, A. Goossens, J. Schooman, *Thin Solid Films* 431-432 (2003) 492-496.
[92] D. S. Su, W. Neumann, M. Giersig, *Thin Solid Films* 361-362 (2000) 218-222.

[93] U. Störkel, M. Aggour, M. Weber, and H.J. Lewerenz, *16th EPVSEC*, 1-5 May 2000, Glasgow, UK.
[94] T. Walter, C. Köble, R. Herberholz and H.W. Schok, *Cryst. Res. Tech.* 31 (1996) 431-434.
[95] F. Qasrawi, N. M. Gasanly, *Crystal Research and Technology*, 38 12, (2003) 1063-1070.
[96] Klug, Harold P., and Alexander, Leroy E., 1977, "X-Ray Diffraction Procedures for Polycrystalline and Amorphous Materials", Second Edition, John Wiley, 966 p.
[97] A. Antony, A. S. Asha, R. Yoosuf, R. Manoj, M. K. Jayaraj, *Sol. En. Mat. Sol. Cells*, 81 (2004) *407-417*
[98] R. R. Philip, B. Pradeep, G. S. Okram, V. Ganesan, *Semicond. Sci. Technol*., 19, (2004) 798
[99] S. Siebentritt, and S. Schuler, *J. Phys. Chem. Solids*, 64 (2003) 1621.
[100] Y.B. He, T. Krämer, A. Polity, R. Gregor, W. Kriegseis, I. Österreicher, D. Hasselkamp, and B.K. Meyer, *Thin Solid Films*, 431-432 (2003) 231.
[101] Shoji Kitamura, Saburo Endo and Taizo Irie, *Journal of Physics and Chemistry of Solids* 46, 8 (1985) 881-885.
[102] M. Abaab, M. Kanzari, B. Rezig, and M. Brunel, *Sol. En Mat. Sol. Cells*, 59 (1999) 299.
[103] T. Walter, R. Herberholz, C. Müller, H. W. Schock, *J. Appl. Phys.*, 80 (1996) 4411.
[104] M.C. Zouagi, T.B. Nasrallah, M. Amlouk, S. Belgacem, *Proc. 19th EUPVSEC Conf.* 7-11 June 2004, Paris France, 1964-1767.
[105] P. Zabierowski, U. Rau, M. Igalson, *Thin Solid Films* 387 (2001) 147-150.
[106] M. Krunks, E. Mellikov, *Thin Solid Films* 270 (1995) 33-36.
[107] I. Oja, A. Mere, M. Krunks, C.-H. Solterbeck, M. Es-Souni. *Solid State Phenomena*, 99-100 (2004) 259-264.
[108] Krunks, M., Bijakina, O., Mellikov, E., & Varema, T. *Ternary and Multinary Compounds*, 152 (1998) 325-328.
[109] F.–J. Haug, D. Rudmann, G. Bilger, H. Zogg, A. N. Tiwari) *Thin Solid Films* 403-404 (2002) 293-296.
[110] O. Kijatkina, M. Krunks, A. Mere, B. Mahrov, L. Dloczik, *Thin Solid Films*, 431-432 (2003) 105-109.
[111] H. Bozouita, N. Bouguila, A.Dhouib, *Renewable Energy* 17 (1999) 85-93.
[112] U. Rau, H. W. Schock, *Applied Physics* A 69, 131 (1999).
[113] J. Verschraegen, M. Burgelman, J. Penndorf, *Thin Solid Films* 480-481, (2005) 307-311
[114] M. Rusu, W. Eisele, R. Würz, A. Ennaoui, M. Ch. Lux-Steiner, T. P. Niesen, F. Karg, *Journal of Physics and Chemistry of Solids* 64 (2003) 2037-2040.
[115] R. Herberholz, M. Igalson, H. W. Schock, *J. Appl. Phys.* 83 (1) (1998) 318-325.

Appendix

Article I

M. Krunks, V. Mikli, O. Bijakina, H. Rebane, A. Mere, T. Varema, E. Mellikov, Composition and structure of $CuInS_2$ films prepared by spray pyrolysis, *Thin Solid Films*, 361-362 (2000) 61-64.

Appendix

Article II

M. Krunks, O. Kijatkina, J. Blums, I. Oja, **A. Mere**, E. Mellikov, Cost-effective sprayed $CuInS_2$ films for solar cells, Proceedings 17-th European PVSEC, Oct. 22-26 2001, Munich, Germany, *published by WIP-Munich and ETA-Florence*, v. 2 (2002) 1211-1214.

Appendix

Article III

A. Mere, O. Kijatkina, H. Rebane, J. Krustok, M. Krunks, Electrical properties of sprayed $CuInS_2$ films for solar cells, *J. Phys. Chem. Solids*, 64 (2003) 2025-2029.

Appendix

Article IV

A. Mere , A. Katerski, O. Kijatkina, M. Krunks, 2004, Solar Cell Structures by Non-Vacuum Techniques Based on Sprayed $CuInS_2$ Absorber Layers. – *Proceedings 19-th PVSEC*, June 7-11, 2004, Paris, 1973-1976.

Appendix

Article V

M. Krunks, O. Kijatkina, **A. Mere**, T. Varema, I.Oja, V. Mikli, Sprayed $CuInS_2$ films grown under Cu-rich conditions as absorbers for solar cells, *Solar Energy Materials and Solar Cells*, 87 (2005) 207-214.

Appendix

Article VI

I. Oja, M. Nanu, A. Katerski, M. Krunks, **A. Mere**, J. Raudoja, A. Goossens, Crystal quality studies of $CuInS_2$ films prepared by spray pyrolysis, *Thin Solid Films*, 480-481 (2005) 82-86.

Appendix

Article VII

M. Krunks, **A. Mere**, A. Katerski, V. Mikli, J. Krustok, Characterisation of sprayed $CuInS_2$ films annealed in hydrogen sulphide atmosphere, *Thin Solid Films*, 2006, available online from Jan.19, 2006, at http.//www.sciencedirect.com/.

Appendix

Article VIII

M. Krunks, **A. Mere**, O. Kijatkina, Solar Cell Based on $CuInS_2$ Absorber Layer Prepared by Chemical Spray Pyrolysis, *United States Patent Application Publication No: US 2005/0271827 A1, Dec. 8, 2005.*